UCRL-ID-131166

Isothermal Fatigue

D. Lesuer
C. Syn

June 1998

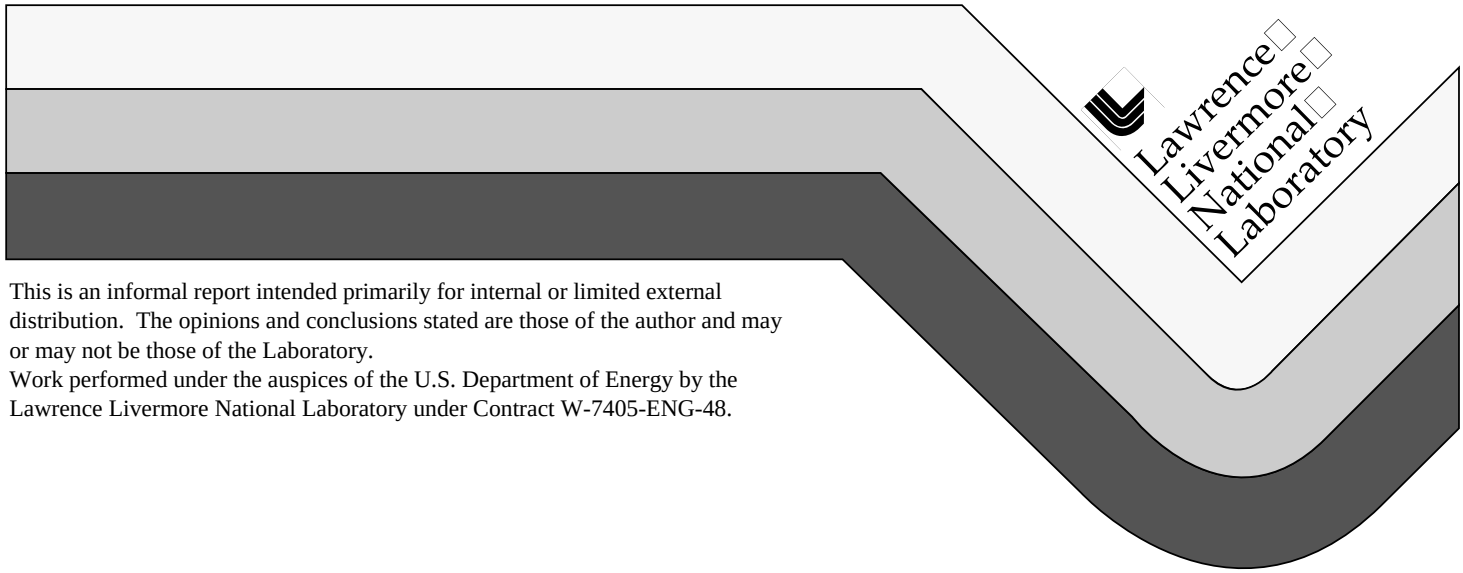

Work performed under the auspices of the U.S. Department of Energy by the Lawrence Livermore National Laboratory under Contract W-7405-ENG-48.

Lightweight Materials for Automotive Applications
CRADA TC-0296-92-B
between General Motors Research and Development Center and
Lawrence Livermore National Laboratory
Topic 3 Metal Matrix Composites
Fatigue Subtask

Isothermal Fatigue

Don Lesuer and Chol Syn
Lawrence Livermore National Laboratory
Livermore, CA 94551

ABSTRACT

Metal matrix composites consisting of the 339 aluminum casting reinforced with Kaowool have been studied for their high cycle fatigue behavior. This report describes results and data analysis for the 339/Kaowool/15w composite. The project involved testing 130 339/Kaowool/15w samples at different temperatures from room temperature to 300°C. Experiments were conducted on samples that had received different annealing treatments before testing. The defects responsible for fatigue failure were characterized. In the high cycle fatigue regime, the number of cycles to failure was found to vary as a power law function of the stress. Sufficient data were available for failures originating from three different defect / testing temperature combinations to quantify the relationship between defect type, defect size and cycling stress on resulting fatigue life. The three defect type / testing temperature combinations were shot particles at 200°C, porosity at 200°C and shot particles at 300°C. A new model was proposed to predict the life of samples as a function of stress and defect characteristics (size and type). For the three data sets described above, the model could predict the life of the three different defect / temperature combinations described above to better than half a decade.

INTRODUCTION

The isothermal, high cycle fatigue behavior of two metal matrix composites (339/Kaowool/7w[1] and 339/Kaowool/15w) and the matrix alloy (339 aluminum casting alloy) has been evaluated at room temperature and elevated temperature. Axial fatigue tests were performed. The failure initiation sites were then identified and the microstructural features participating in the fatigue process were analyzed. Most of the work was done on the 339/Kaowool/15w composite. During the project, 130 339/Kaowool/15w samples were tested, and, for most of these samples, the fracture surfaces were characterized. Samples were annealed and tested at a number of different temperatures. This report is concerned with the mechanism of fatigue failure at 200°C and 300°C. For most of the samples, the failure origin and defects responsible for fatigue failure could be established. The data was analyzed with the intent of quantifying the relationship between defect type, defect size and cycling stress on the resulting fatigue life.

MATERIALS AND EXPERIMENTAL PROCEDURES

Materials.

Work was completed on three different types of 339/Kaowool/15w composite. The materials differ in the cleaning processes used to remove objectionably large particles from the ceramic reinforcement before pre-form fabrication. The reinforcement resulting from these three cleaning processes are referred to as high shot, low shot and Didier cleaned. The high shot material had no cleaning of the reinforcement prior to pre-form fabrication. The low shot material was cleaned by Thermal Ceramics Inc. prior to pre-form fabrication. The Didier-cleaned material was cleaned by a French firm prior to pre-form fabrication using a proprietary process.

Work by General Motors (GM) has established that overaging of the matrix can result from annealing the 339/Kaowool composites at the testing temperatures (200°C and 300°C). This matrix overaging can produce significant reductions in fatigue life. Therefore, all data analyzed in this report was on done on material annealed at the testing temperature for 200 hours (time required for 10^7 cycles) prior to fatigue experiments. These annealing treatments overaged the matrix of the composite and thus eliminated the softening of the matrix that occurs with time in a fatigue test as a factor in analysis of fatigue life.

[1] This report specifies MMCs according to a system established by the Aluminum Association. This five part system designates the composite by aluminum alloy, reinforcement material, volume percentage reinforcement, reinforcement morphology and matrix alloy temper.

Disks of the composite were squeeze cast by GM. The castings were then aged for 8 hours at 210°C to produce a T5 temper in the matrix prior to the machining of cylindrical samples. Samples were pre-aged by LLNL at the intended testing temperature for 200 hours. The gage section of all samples was polished by GM or LLNL. For the GM-polished samples, this procedure was completed before the pre-aging treatment. For the LLNL-polished samples, this procedure was completed after the pre-aging treatment. No difference in failure origins or fatigue data was observed between the LLNL- and GM-polished samples. The polishing procedure used by LLNL and the resulting surface finish have been documented in a previous report [1]. An optical micrograph of the 339/Kaowool/15w composite is shown in Fig. 1.

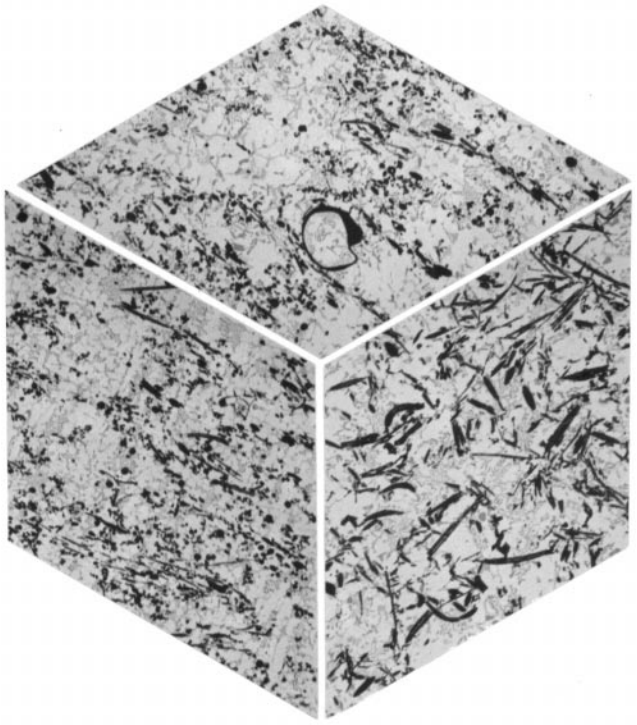

Fig. 1. Optical micrograph of the 339/Kaowool/15w composite.

Testing and fracture surface examination.

Axial fatigue tests were conducted in air with an MTS servohydraulic system and MTS hydraulic grips containing wedge jaws. All testing was done using fully reverse loading (R = -1) under load control (sinusoidal waveform) with an operating frequency of 20 Hz. Cycling stresses were chosen to provide data primarily in the high cycle fatigue regime ($> 10^5$ cycles to failure).

Fatigue fractured samples were examined using SEM to locate the fatigue failure initiation site and characterize the flaw that initiated failure. The matching fracture surfaces of each broken sample were coated with a thin layer of Au-Pd and photographed at a low magnification (25X to 50X) first to locate the origin of the fatigue crack, and then at higher magnifications (up to 5000X) to determine the shape and size of the flaw at the origin. On some samples, X-ray energy dispersive spectrometry

(EDS) was performed to identify the chemical composition of the flaw at the origin. The relative location of the flaw with respect to the sample surface was also measured and tabulated with other information on the fatigue test and the nature of the crack initiating flaw of each sample.

Most of the fatigue failures initiated at porosity or shot particles. Typical orgins are shown in Figs. 2 and 3 for porosity or shot-initiated failures respectively.

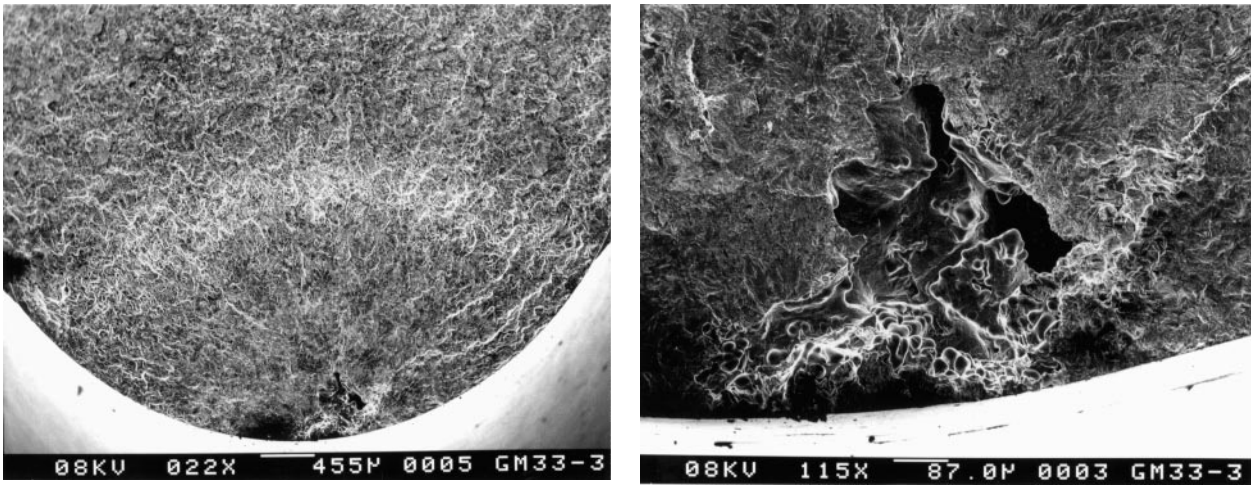

a b

Fig. 2. Typical fatigue failure origin resulting from porosity. Sample is the 339 matrix alloy tested at 20°C. Fracture surface is shown at low (a) and high magnification (b).

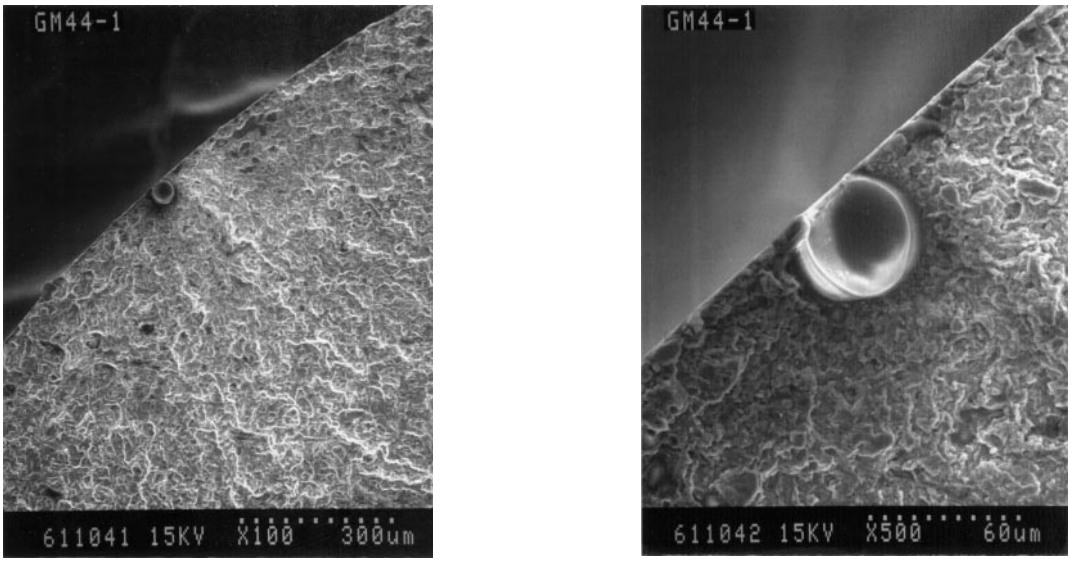

a b

Fig. 3. Typical fatigue failure origin resulting from a shot particle. Sample is the 339/Kaowool/7w composite tested at 300°C. Fracture surface is shown at low (a) and high magnification (b).

Stress - life behavior.

All the isothermal fatigue data obtained in this project are given in the Appendix, which includes fatigue test results as well as the characteristics of the defect that initiated the fatigue failure. These initiating defects are characterized by defect type, shape, size (dimensions in two orthogonal directions), location (given as a distance below the surface) and the size of the stable fatigue crack growth zone.

Fatigue data for the 339/Kaowool/15w composite manufactured with high shot, low shot and Didier-cleaned reinforcement are shown in Figs. 4, 5 and 6, respectively. Data for the high shot and low shot material are for tests conducted at 20°C, 200°C and 300°C, while data for the Didier-cleaned material are for tests conducted at 200°C and 300°C only. Results are plotted as the maximum stress ($\sigma_{max} = \Delta\sigma / 2$, also referred to as σ) versus number of cycles to failure. All curves in the plots represent the least squares fit of the data to a power law equation using the curve fitting routines in KaleidaGraph (a commercially available data analysis and plotting program). The agreement between the calculated curve and the experimental data is generally very good, which shows that the number of cycles to failure can be represented as a power law function of the stress. This is an important result that will be used in the next section of this report. Figures 4 and 5 show that the σ-N curves at 20°C are much flatter (less change in σ with increasing number of cycles to failure) than the σ-N curves at 200°C in the high shot material and 200°C and 300°C in the low shot material. This seems to be a real effect. The mechanistic origins of this effect, however, are not understood at this time.

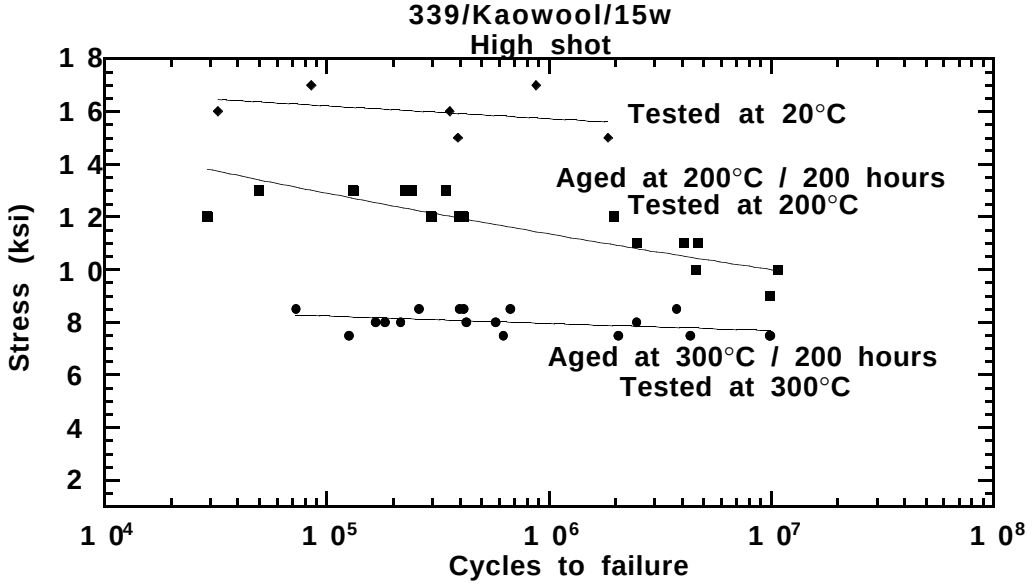

Fig. 4. Stress versus life for the high shot 339/Kaowool/15w composite tested at 20°C, 200°C and 300°C. Samples were pre-annealed at the testing temperature for 200 hours before the fatigue experiments.

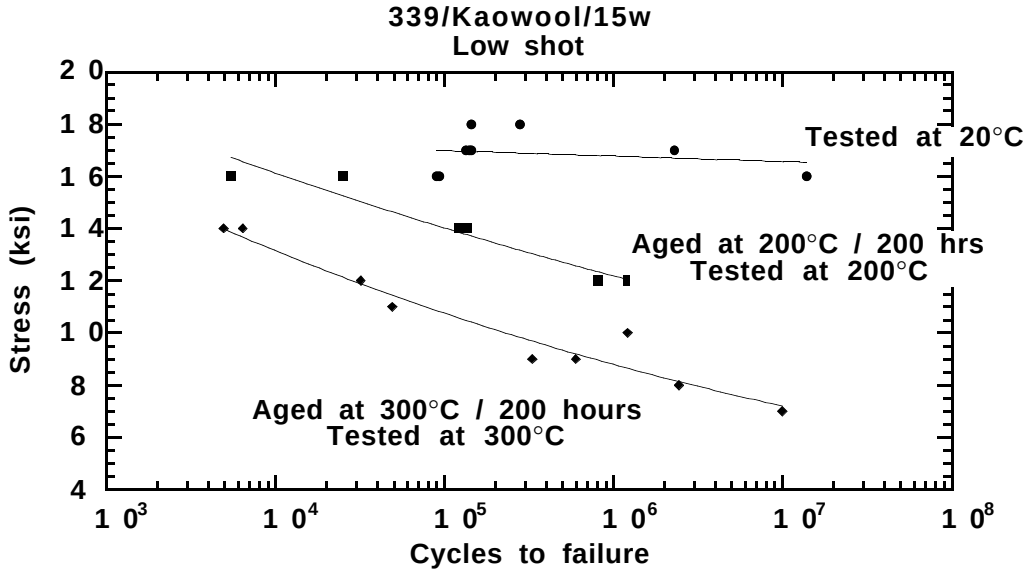

Fig. 5. Stress versus life for the low shot 339/Kaowool/15w composite tested at 20°C, 200°C and 300°C. Samples were pre-annealed at the testing temperature for 200 hours before the fatigue experiments.

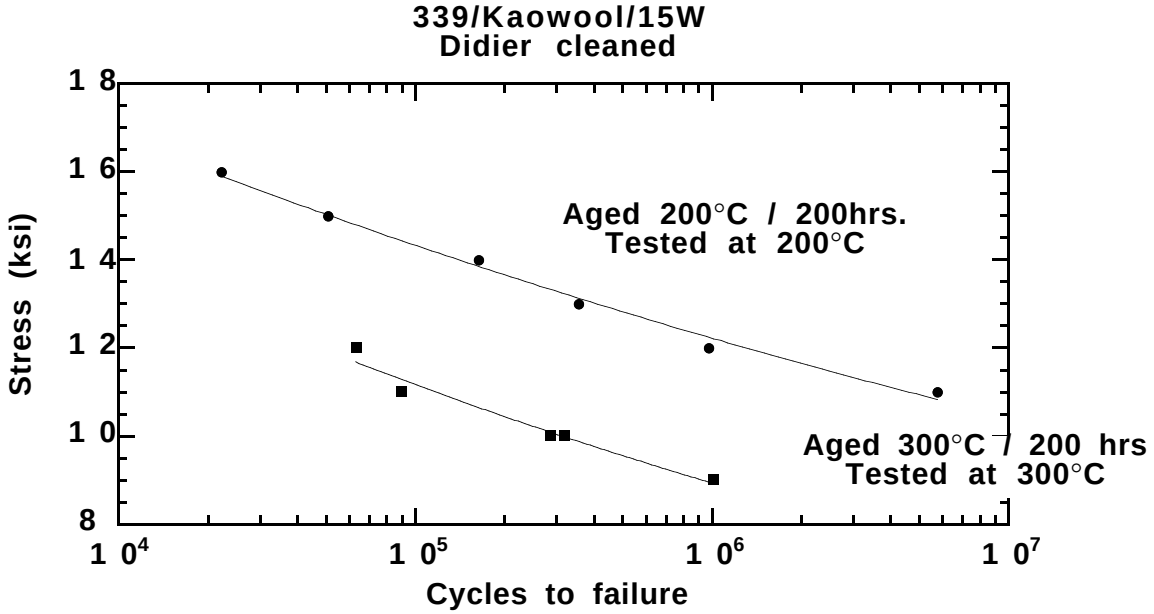

Fig. 6. Stress versus life for the Didier-cleaned 339/Kaowool/15w composite tested at 200°C and 300°C. Samples were pre-annealed at the testing temperature for 200 hours before the fatigue experiments.

All fractures occurred perpendicular to the loading axis. For the high shot and low shot material, the defects initiating failure were almost always shot particles (through fracture of the particle) or porosity. For the Didier-cleaned material, on the other hand, failures were initiated at large pieces of reinforcement or inclusions. In the case of the large reinforcement, both fracture of the reinforcement as well as disbonds between the matrix and the reinforcement were observed.

In Figs. 7 and 8, the σ-N data obtained at 200°C and 300°C respectively are compared for the three types of metal matrix composites (MMCs). At both temperatures, the high shot material had a shorter fatigue life for a given cycling stress than either the low shot or Didier-cleaned material. The low shot and Didier-cleaned materials had very similar lives for a given cycling stress. The difference between the high shot MMC and the low shot / Didier-cleaned MMCs decreases with increasing life until at 10^7 cycles to failure there is very little difference between the fatigue response of all three materials.

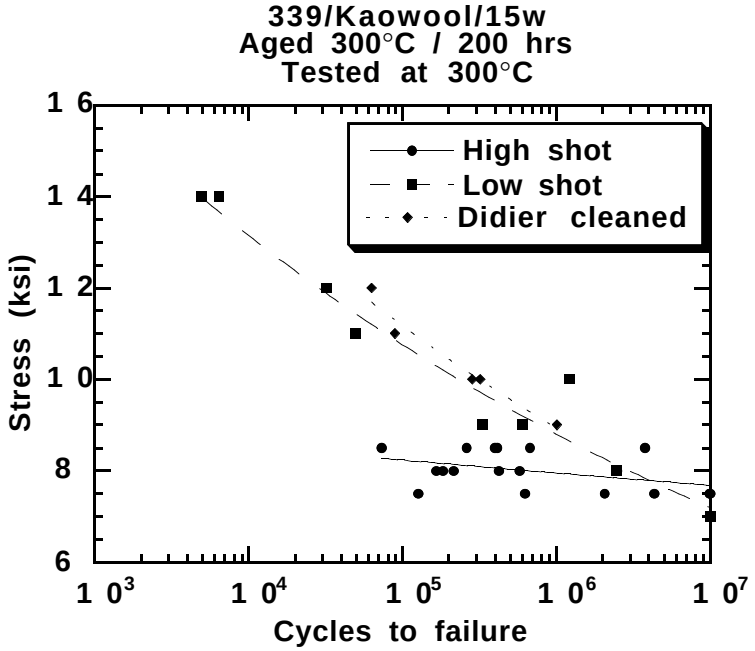

Fig. 7. Stress versus life for high shot, low shot and Didier-cleaned MMC at 300°C.

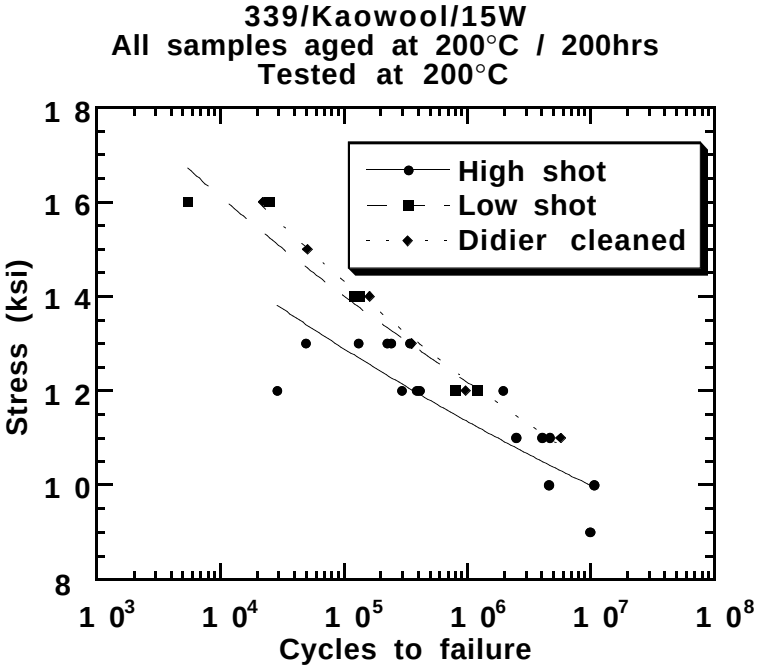

Fig. 8. Stress versus life for high shot, low shot and Didier-cleaned MMC at 200°C.

The data shown in Fig. 4 is replotted in Fig. 9 as log stress versus log cycles to failure. As noted above, the relationship between cycling stress and life can be represented well by a power-law equation in the high cycle fatigue regime. Figure 9 also shows the extrapolation of the power law equation representing the 300°C data to the low cycle fatigue regime. The equation predicts an ultimate tensile strength (stress at 10^0 cycles) of about 9.5 ksi. This strength is significantly less than the UTS measured in a monotonic tensile test of the 339/Kaowool/15w composite that had been aged for 200 hours at 300°C (approximately 20 ksi [2]). The reason for this strength difference is that the tensile and fatigue tests have different failure origins. Failures in the fatigue tests generally initiated from well-defined defects whereas failures in the tensile tests generally could not be associated with a specific defect. This behavior is distinctly different from that observed by Nieh, Lesuer and Syn on the DWA 6090/SiC/25p MMC [3] at room temperature. In the 6090/SiC/25p material, a power-law equation (derived from data in the range of 10^3 to 10^7 cycles to failure) extrapolated to the correct UTS. The origins of faitigue failure, however, are significantly different in the two materials. In 6090/SiC/25p, failures initiated within the matrix, whereas, in 339/Kaowool/15w, failures initiated at defects. It is important to recognize that, in the region of interest (high cycle fatigue), the data can be represented by a power-law equation.

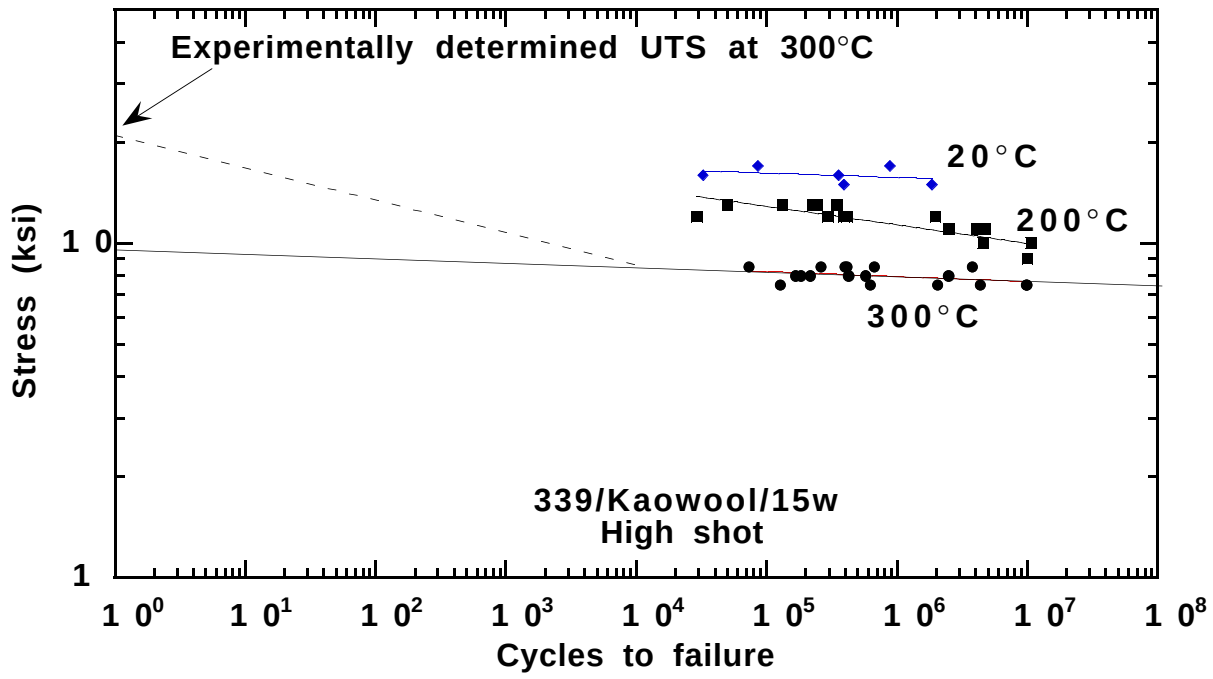

Fig. 9. Stress versus life (plotted on log-log axes) for the high shot 339/Kaowool/15w composite at 20°C, 200°C and 300°C.

Influence of defect type and size .

Background. A number of models have been proposed to describe the influence of defects and stress concentrations on fatigue strength. These models have been recently reviewed by Murakami and Endo [4] and can be loosely classified into three types - (1) models that are based on empirical equations, (2) models that are based on a notch (or stress concentration) factor, and (3) models that are based on fracture mechanics. A fracture mechanics-based model by Murakami and Endo [5] has been used as a reasonable starting point for analysis of the fatigue data reported here. The model relates the fatigue strength to the size of a defect responsible for failure. The model predicts a phenomenological equation of the form

$$\sigma A^{1/n} = C, \qquad (1)$$

where σ is the fatigue strength (taken by Murakami and Endo to be the stress at 10^7 cycles), A is the cross-sectional area of the defect normal to the tensile axis, and n and C are constants. The constant n will be referred to as the area exponent. The correlation between fatigue strength and defect size predicted by Equation (1) was evaluated by Murakami and Endo for a .13%C steel and a .46%C steel. Fatigue strengths were determined in a rotating bending test and a torsion test for samples that had small holes drilled into their surfaces. Excellent agreement was obtained between the predictions of Equation (1) and the experimental data.

As mentioned above, the Murakami and Endo model is based on fracture mechanics - specifically, the influence of the shape and size of an elliptical crack on the stress intensity. The theoretical variation of this maximum stress intensity with area of the defect raised to the 1/4 power is shown in Fig. 10. The maximum stress intensity and the area of the ellipse have been normalized by the stress intensity and area of a circle of unit radius. The dashed lines in the figure show that, for a given aspect ratio, the maximum stress intensity increases as the area of the elliptical crack to the 1/4 power. The results in Fig. 10 have been replotted in Fig. 11 to show more clearly the variation of the maximum stress intensity with defect aspect ratio. This figure will be referred to in the next section. The stress intensity factor shown in Fig. 10 can be assumed to characterize the local stress and strain field in the vicinity of the defect and thus the magnitude of the stress intensity can be related to the local stresses responsible for fatigue crack initiation and growth. Thus, in theory, the n in Equation (1) should be equal to 4.

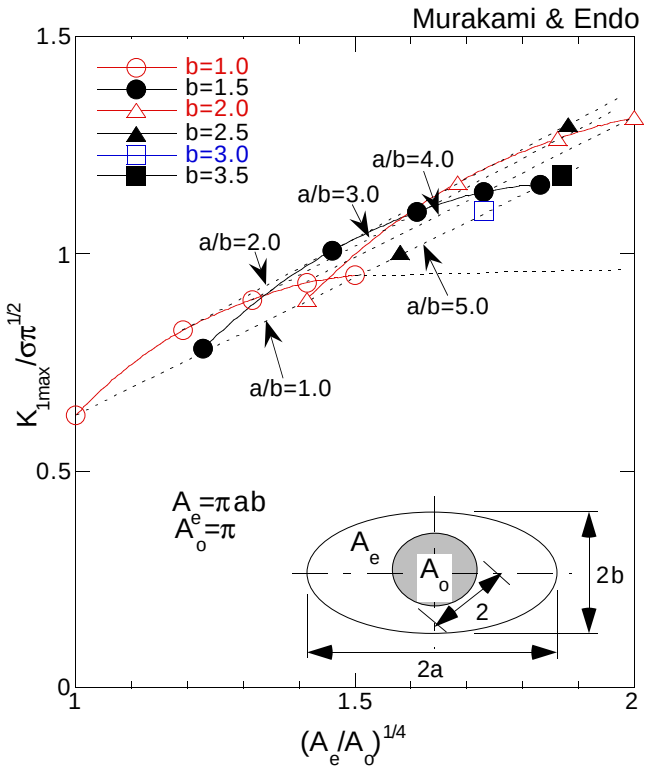

Fig. 10. Normalized maximum stress intensity for an elliptical defect (crack) versus the normalized cross-sectional area of the defect. Maximum stress intensity and the area of the defect have been normalized by the stress intensity and area of a circle of unit radius. Stress intensities are provided for five different crack aspect (a/b) ratios. (after Murakami and Endo [5]).

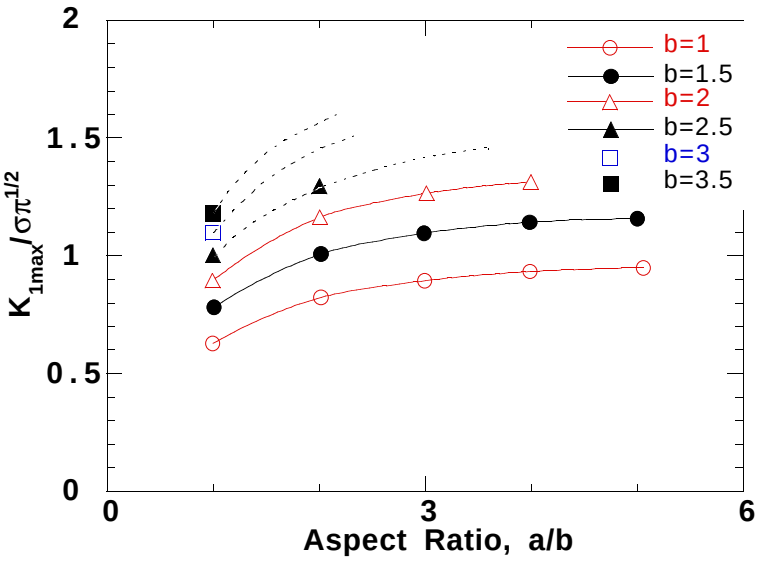

Fig. 11. Normalized maximum stress intensity for an elliptical defect (crack) versus aspect ratio. Data is replotted from Fig. 10.

As discussed in a previous section, there are significant differences in the failure origins observed in the high shot and low shot materials relative to the Didier-cleaned material. We have focused on the data sets resulting from the high shot and low shot materials and have applied Equation (1) to these data. Sufficient data were available for failures originating from shot particles and porosity at 200°C and shot particles at 300°C to make a valid assessment of Equation (1). We have evaluated Equation (1) for a fatigue strength defined at 10^7 cycles as well as 10^5 cycles.

Shot particles - 200°C. Fatigue data are plotted in Fig. 12 for 339/Kaowool/15w samples tested at 200°C that had failures initiating at shot particles. It is important to recognize that all the 339/Kaowool/15w data in the Appendix for low and high shot material with shot particle-initiated failures at 200°C are shown in the figure.

The local stress intensity and σ-N response of the 339/Kaowool composites are influenced by the characteristics of the defect structure. For shot particles (as well as porosity), the most significant characteristics are defect shape, location and size. These characteristics are noted for each data point in Fig. 12 as the dimensions of the shot particle (in μm), its location below the surface (in μm), and the cross-sectional area (in μm^2). The cross sectional area (A) was calculated from the dimensions, assuming an ellipse, using the formula

$$A = \pi ab, \qquad (2)$$

where a and b are 1/2 the major and minor axes, respectively, as shown for the ellipse provided in the inset drawing of Fig. 10. Examination of the defect data in Fig. 12 shows that the location and aspect ratio of the shot particles are not significant variables in the fatigue data. This conclusion is based on the following three observations. (a) All shot particles were located at or near the surface. (All "near surface" particles were located significantly less than the radius of the particle from the surface.) (b) The aspect ratio (b/a in Fig. 10) varies from 1 to 2.5, which can introduce an uncertainty in K_{max} of about 30%, as shown in Fig. 11. (c) The defect area varies by over a factor of two, which can produce a change in K_{max} of over a factor of two. Thus the most significant variable that influences the σ-N behavior in this study is defect size, and the data in Fig. 12 will be analyzed relative to this variable.

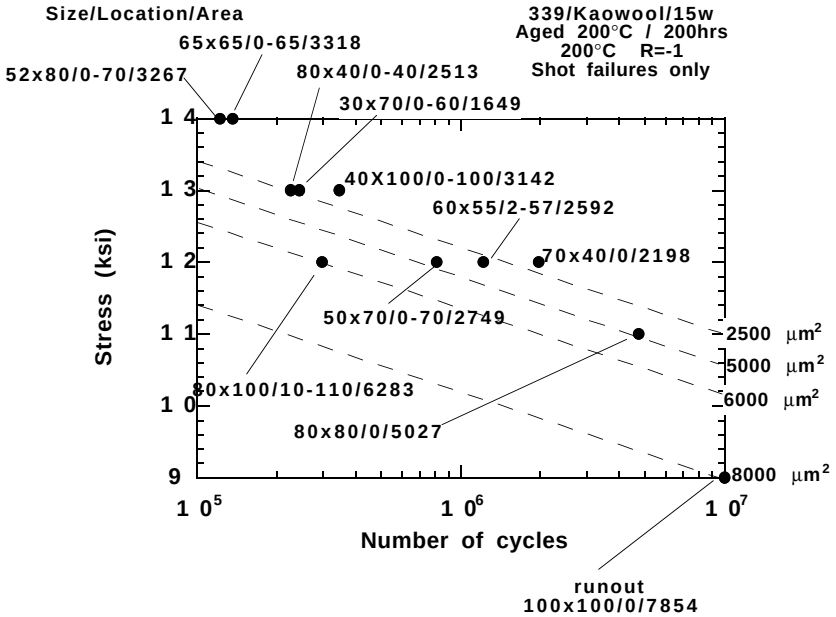

Fig. 12. Stress versus number of cycles for 339/Kaowool/15w samples with failures originating from shot particles. Samples were tested at 200°C. The size, location and area of the shot particles initiating failure are indicated. Curves have been constructed to show the σ-N response expected for defects of a given cross-sectional area.

Based on the data points given in Fig. 12, σ-N curves were constructed for defects of constant size. These curves were constructed for defect areas equal to 2500 μm^2, 5000 μm^2, 6000 μm^2 and 8000 μm^2. The fatigue strengths at 10^5 and 10^7 cycles to failure were then plotted as a function of defect area. The results are given in Fig. 13 and show that the fatigue strength at both 10^5 and 10^7 cycles can be represented as a power law function of the defect area as predicted by Equation (1). The area exponent (n) from Equation (1) for the 200°C shot particle failures is given in Table I and compared with n exponents from other studies. In all cases, the n value is larger than the theoretical value of 4. Thus the local stress intensity is not as high as the theoretical prediction. Murakami and Endo observed this deviation from theory and attributed it to crack length effects and the difference between "small and large-scale yielding". For all the defects shown in Table I, the defect sizes are small enough that the material can no longer be treated as a continuum (as assumed in the analysis of Fig. 10) and short crack effects must be considered.

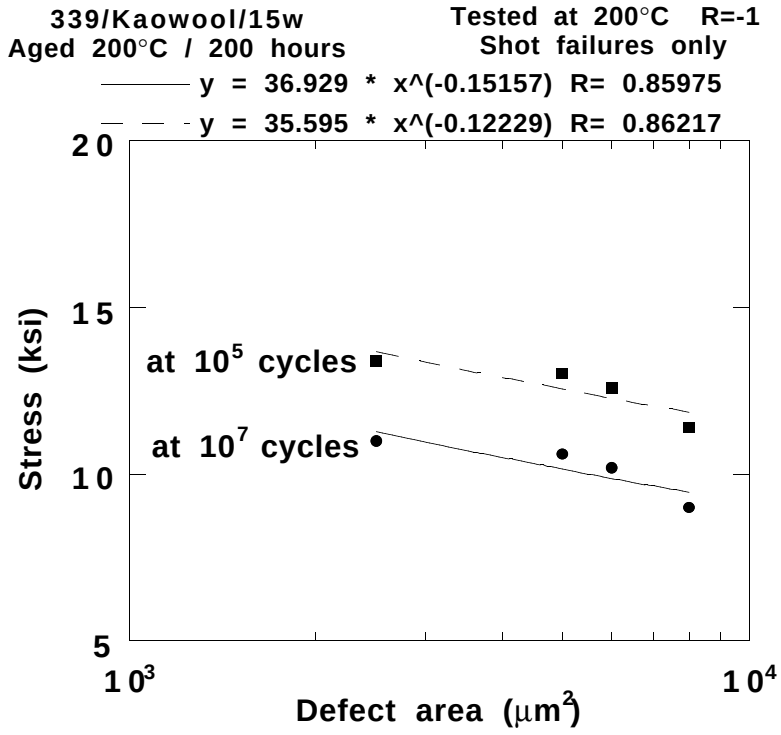

Fig. 13. Fatigue strength at 10^5 and 10^7 cycles versus defect area for 339/Kaowool/15w with failures due to shot particles at 200°C. Lines represent a power law fit to the data.

Table I
Area Exponent (n) from Equation (1)

Material	Defect type	Range in defect size (μm)[1]	Testing temperature (°C)	Testing method	n	Reference
.46%C steel	drilled holes	40 - 500	20	bending	12.0	5
.13%C steel	drilled holes	40 - 500	20	bending	11.2	5
.46%C steel	drilled holes	40 - 500	20	torsional	13.4	5
.39%C steel	irregular drilled holes		20	bending	4.6	5, 6
.39%C steel	irregular drilled hole		20	torsional	7.2	5, 6
.46%C steel	unknown		unknown	rotating bending	5.2	5, 7
.46%c steel	unknown		unknown	rotating bending	8.0	5, 7
339/Kaowool/15w	shot particles	40 - 100	200	axial	6.6	present study (Fig. 13)
339/Kaowool/15w	shot particles	40 - 100	200	axial	13.0	present study (Fig. 16)
339/Kaowool/15w	porosity	50 - 350	200	axial	13.8	present study (Fig. 20)
339/Kaowool/15w	porosity	50 - 350	200	axial	24.3	present study (Fig. 23)
339/Kaowool/15w	shot particles	20 - 160	300	axial	9.0	present study
2124/SiC/20p-T6	SiC particles	3 - 35	20	axial	11.8	present study (data from ref. 9)

The model presented by Murakami and Endo relates fatigue strength to defect size. The area exponent (n) and constant (C) in Equation (1) characterize the local stress intensity resulting from shot particles at 200°C. This characterization of the stress intensity can be used in a new model that can predict the life of samples as a function of stress and defect characteristics (size and type). The model is based on the well-established empirical equation [8] relating the maximum stress ($\sigma = \Delta\sigma/2$) and life (N), namely,

$$N = C_1\sigma^p, \tag{3}$$

where C_1 and p are experimentally determined constants. The model assumes that a similar power-law equation relates N and K_{max} (also referred to as K). Thus

$$N = C_2K^q, \tag{4}$$

where q and C_2 are constants. Since K varies as $\sigma A^{1/n}$ in Equation (1), Equation (4) can be written as

$$N = C_3(\sigma A^{1/n})^q, \tag{5}$$

[1] taken as the minimum and maximum dimensions observed in the data.

where C_3 is again a constant. The data in Fig. 12 has been analyzed using Equation (5) and the value of n determined in Fig. 13. Results are shown in Fig. 14, in which the life is plotted against the local stress intensity for shot particles tested at 200°C. The plot shows that the fatigue data, which includes cycling stress as well as defect area, can be represented well by Equation (5).

The life equation for shot failures at 200°C in the 339/Kaowool/15w composite is given by

$$N = 3.83\ 10^{26}\ (\sigma A^{.15})^{-12.9} \qquad (6)$$

The life calculated from this equation, assuming a range of cycling stresses and defect areas observed in this study, is compared in Fig. 15 with the life obtained experimentally. As can be seen, the agreement is excellent; the equation can predict life to better than half a decade. It should be mentioned that all the data in the Appendix for shot failures at 200°C (including low shot and high shot, pre-aged material - 12 data points) are given in the figure.

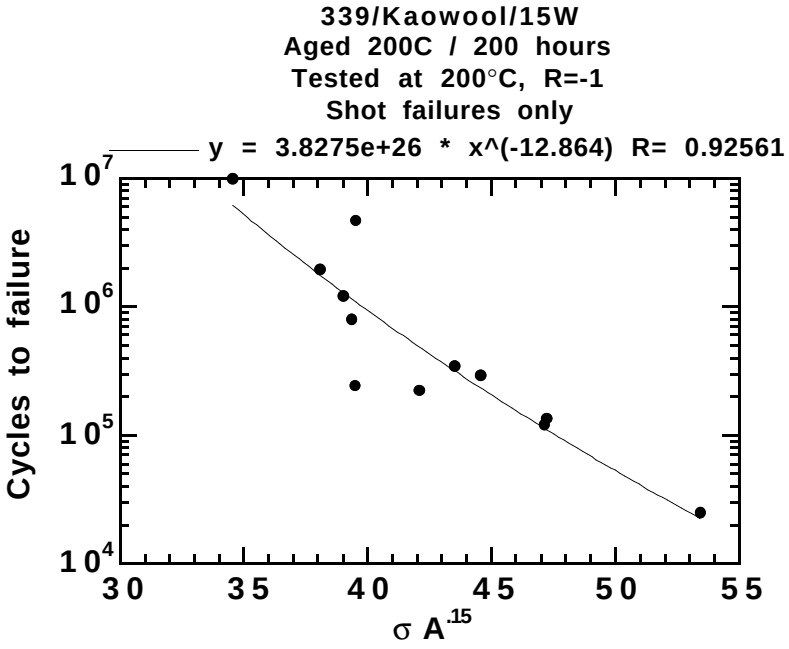

Fig. 14. Cycles to failure versus local stress intensity for shot failures at 200°C. Local stress intensity ($\sigma A^{.15}$) is derived from the analysis in Fig. 13. Line represents a power law fit to the data.

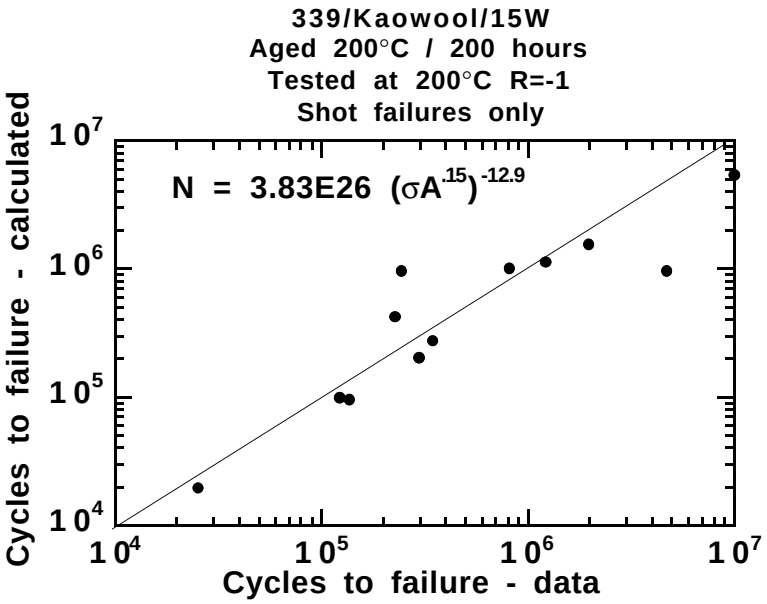

Fig. 15. Calculated number of cycles to failure versus experimental data. Calculations are based on the equation shown in the figure.

Further analysis of the data in Fig. 13 suggests that there may be breaks in the stress - defect area curves as shown in Fig. 16. Each curve has two segments with different area exponents. A change in area exponent with decreasing defect area might be expected, since at small defect sizes, short crack effects can be expected to be observed. As noted earlier, the n value is significantly larger than the theoretical value of 4 at these small defect sizes. It is interesting to note that the break in the curve results in an n value at large defect sizes that approaches 4 (the value predicted by fracture mechanics). Thus the results in Fig. 16 suggest that at large defect sizes long crack effects are obtained and the material can be treated as a continuum with n approximately equal to 4. At small defect sizes, short crack effects are observed and the n values are significantly larger than 4.

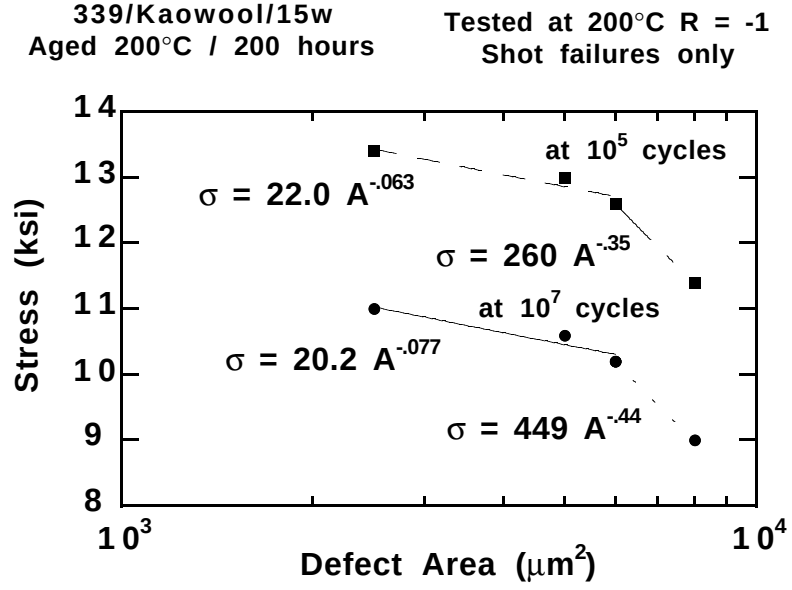

Fig. 16. Analysis of the data in Fig. 13 showing a break in the curve at defect size equal to 6,000 μm^2.

We have analyzed all the data in Fig. 14 as previously described using Equation (5). The area exponent at small defect sizes was used in the analysis, since most of the data (with the exception of 2 data points) had defect sizes less than 6000 μm^2. The results are shown in Figs. 17 and 18. The life equation obtained from this analysis was

$$N = 1.17\ 10^{23}\ (\sigma A^{.077})^{-12.7} \qquad (7)$$

Agreement between calculated life and experimental data is excellent with the equation predicting life to better than half a decade.

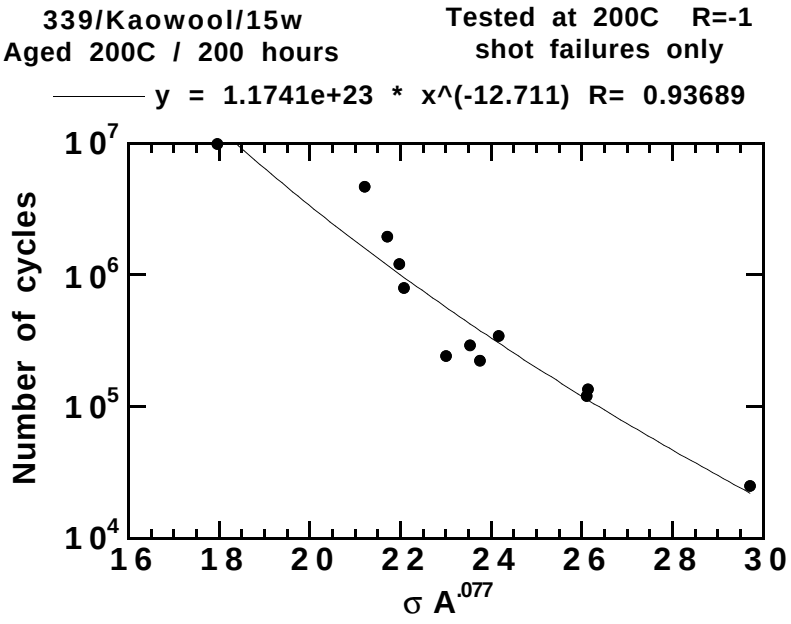

Fig. 17. Cycles to failure versus local stress intensity for shot failures at 200°C. Local stress intensity ($\sigma A^{.077}$) is derived from the analysis at small defect sizes (less than 6,000 μm^2) in Fig. 16. Line represents a power law fit to the data.

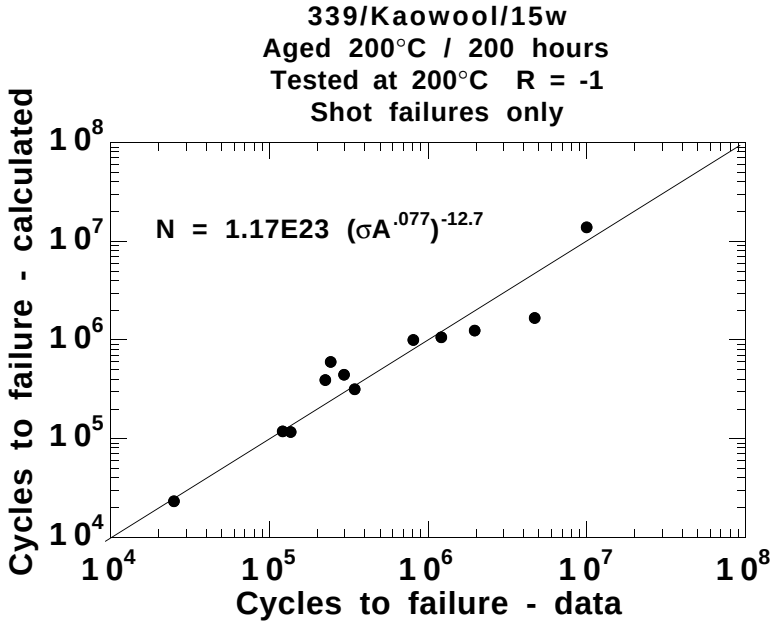

Fig. 18. Calculated number of cycles to failure versus experimental data. Calculations are based on the equation shown in the figure.

Porosity - 200°C. The fatigue data for porosity-initiated failures at 200°C was analyzed using the same methodology as the data above. The results are shown in Fig. 19 and σ-N curves for defects of constant size were constructed for porosity areas of 2500 μm^2, 10,000 μm^2, 14,000 μm^2 and 28,000 μm^2. It is important to recognize that all the 339/Kaowool/15w data in the Appendix with porosity-related failures at 200°C are shown in the figure. The fatigue strengths at 10^5 and 10^7 cycles are plotted versus defect area in Fig. 20 and reasonable agreement is obtained with Equation (1). The area exponent (n), recorded in Table I, is 13.8 and is larger than the n obtained from shot particles in the 339/Kaowool/15w composite or from the drilled holes in the data analyzed by Murakami and Endo. This result indicates that the local stress intensity resulting from porosity is a weaker function of defect area than the stress intensity resulting from other defects. This effect is caused by differences in the two types of defects. Porosity has ligaments spanning the defect region, whereas the shot and drilled holes do not. The ligaments present in the porosity defects are load bearing and reduce the local stress intensity experienced by the most highly stressed region of the defect. The result is that at large defect sizes, porosity is less damaging than shot for defects of the same cross-sectional area.

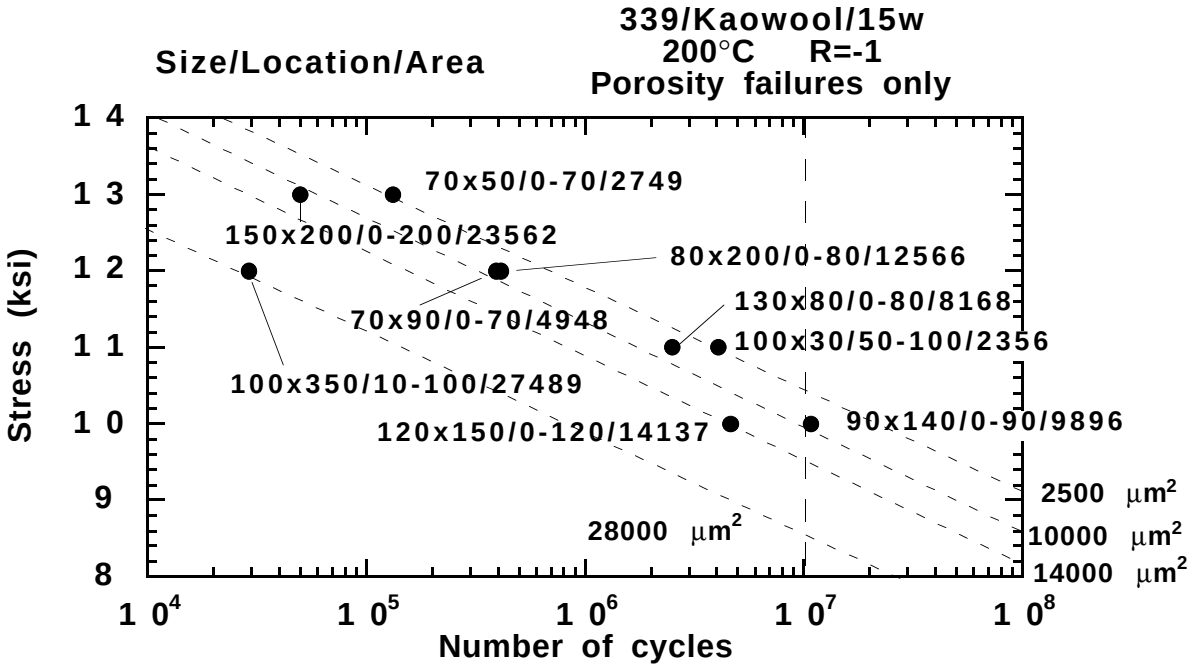

Fig. 19. Stress versus number of cycles for 339/Kaowool/15w samples with failures originating from porosity. Samples were tested at 200°C. The size, location and area of the porosity regions initiating failure are indicated. Curves have been constructed to show the σ–N curves expected for defects of a given cross-sectional area.

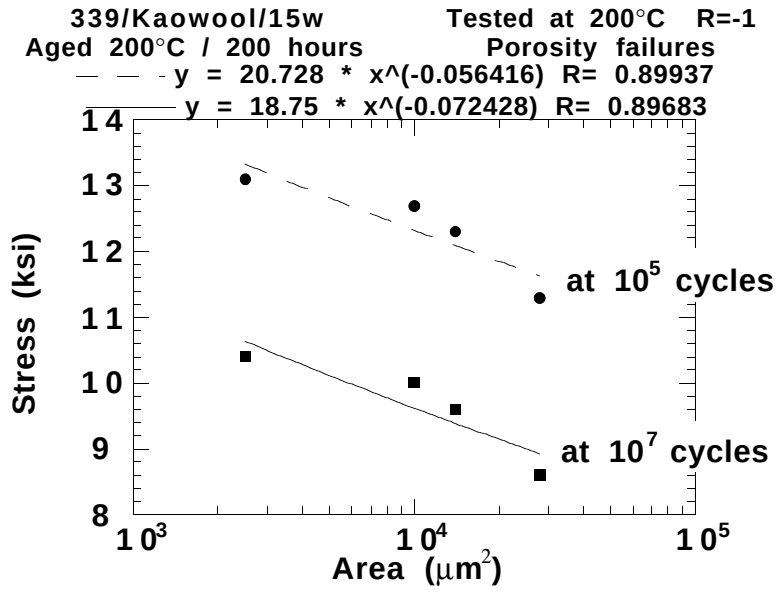

Fig. 20. Fatigue strength at 10^5 and 10^7 cycles versus defect area for 339/Kaowool/15w with failures due to porosity at 200°C. Lines represent a power law fit to the data.

The porosity data at 200°C were evaluated according to Equation (5) using the area exponent recorded in Table I. The results are shown in Fig. 21 for the nine porosity failures observed in pre-aged samples at 200°C. As with the shot failures at 200°C, Equation (5) represents well the variation of life with the local stress intensity. This equation is

$$N = 7.27\ 10^{28}\ (\sigma A^{.072})^{-17.2} \qquad (8)$$

The life predicted by this equation is compared with experimental data in Fig. 22. With the exception of one data point, calculated values differ from experimental values by at most half a decade.

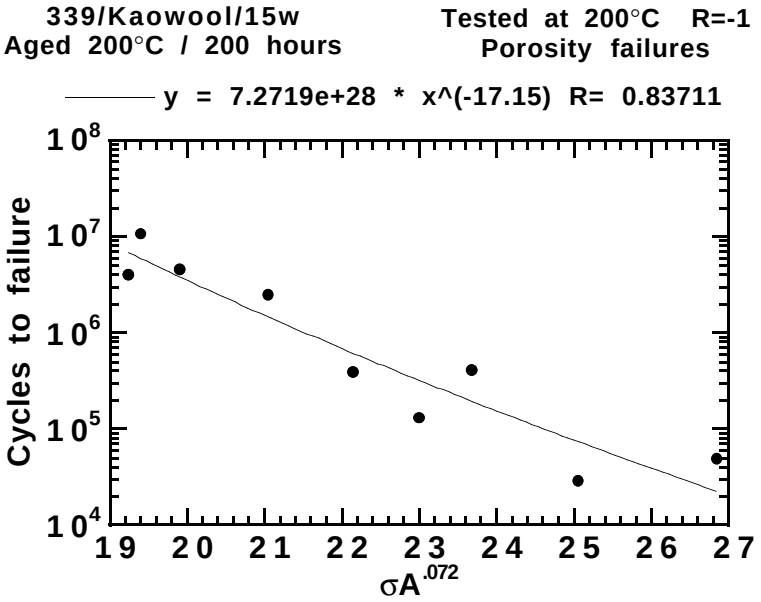

Fig. 21. Cycles to failure versus local stress intensity for porosity failures at 200°C. Local stress intensity ($\sigma A^{.072}$) is derived from the analysis in Fig. 14 . Line represents a power law fit to the data.

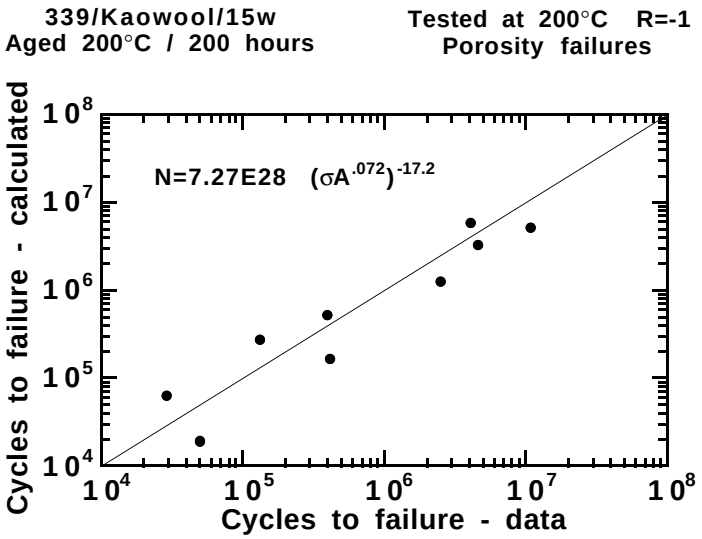

Fig. 22. Calculated number of cycles to failure versus experimental data. Calculations are based on the equation shown in the figure.

Further analysis of the data in Fig. 20 suggests that, as with the 200°C shot failure data, there may be a break in the stress - defect area curve as shown in Fig. 23. Thus the data for both 10^5 cycles and 10^7 cycles can be represented by two line segments (with two different area exponents) as shown in the figure. We have anaylyzed all the data in Fig. 14 as previously described using Equation (5). As with the 200°C shot failure data, we have used the area exponent for the curve segment at small defect sizes (less than 14,000 μm^2), since most of the data results from defects that are less than 14,000 μm^2. The results are shown in Figs. 24 and 25. The life equation obtained from this analysis was

$$N = 2.85\ 10^{29}\ (\sigma A^{.041})^{-19.3} \qquad (9)$$

Agreement between calculated life and experimental data is excellent with the equation predicting life to better than half a decade.

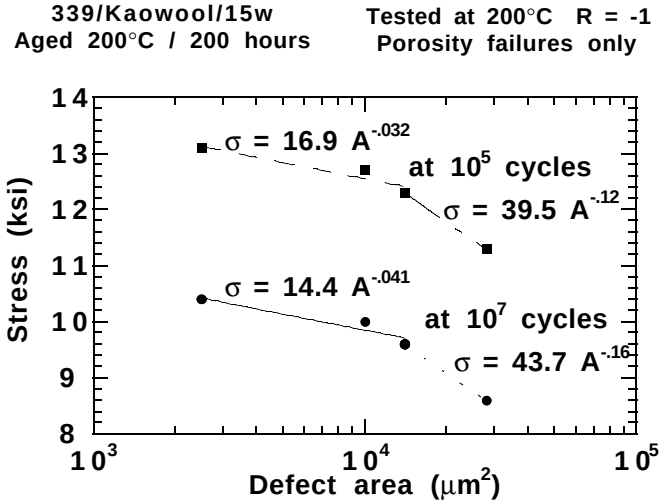

Fig. 23. Analysis of the data in Fig. 20 showing a break in the curve at defect size equal to 14,000 μm^2.

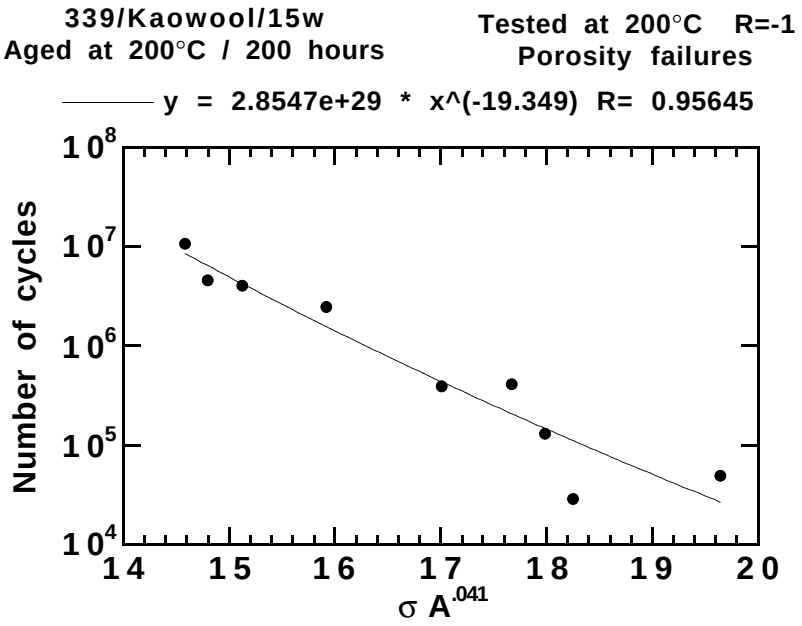

Fig. 24. Cycles to failure versus local stress intensity for porosity failures at 200°C. Local stress intensity ($\sigma A^{.041}$) is derived from the analysis at small defect sizes (less than 14,000 μm^2) in Fig. 23. Line represents a power law fit to the data.

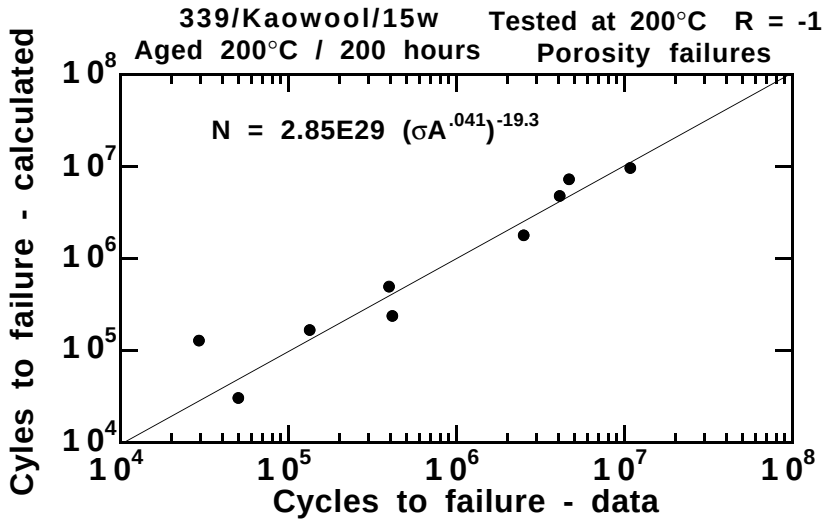

Fig. 25. Calculated number of cycles to failure versus experimental data. Calculations are based on the equation shown in the figure.

Shot particles - 300°C. The fatigue data for shot-initiated failures at 300°C were analyzed using the same methodology as the 200°C data for shot and porosity failures. Ten samples were suitable for analysis and the results are reported in Figs. 26 - 29. The fatigue strengths at 10^5 and 10^7 cycles to failure are plotted against defect area in Fig. 27 and the results show reasonable agreement with Equation (1).

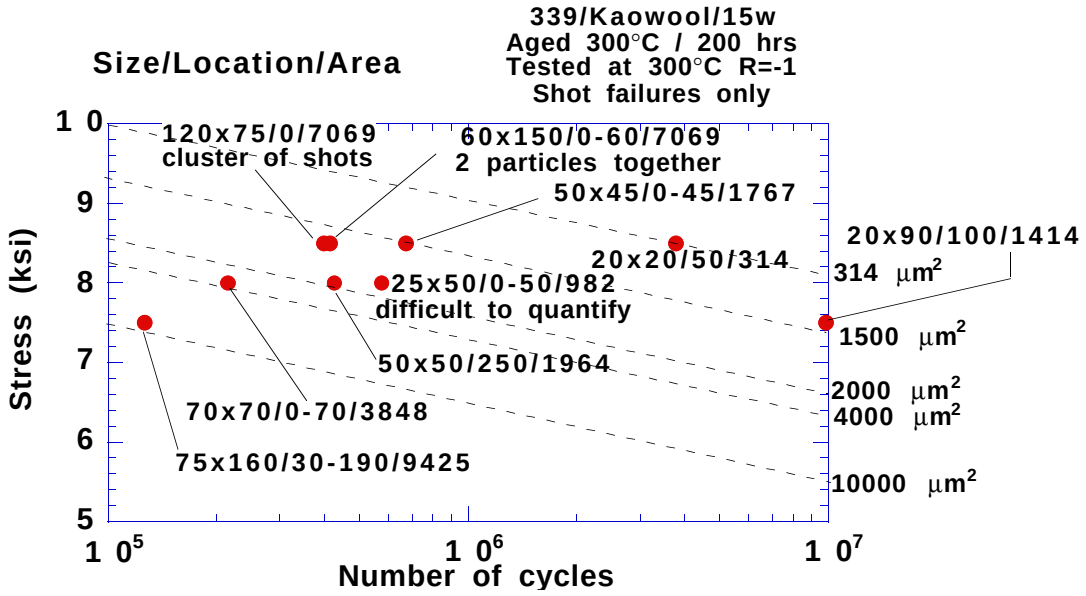

Fig. 26. Stress versus number of cycles for 339/Kaowool/15w samples with failures originating from shot particles. Samples were tested at 300°C. The size, location and area of the shot particles initiating failure are indicated. Curves have been constructed to show the σ–N curves expected for defects of a given cross-sectional area.

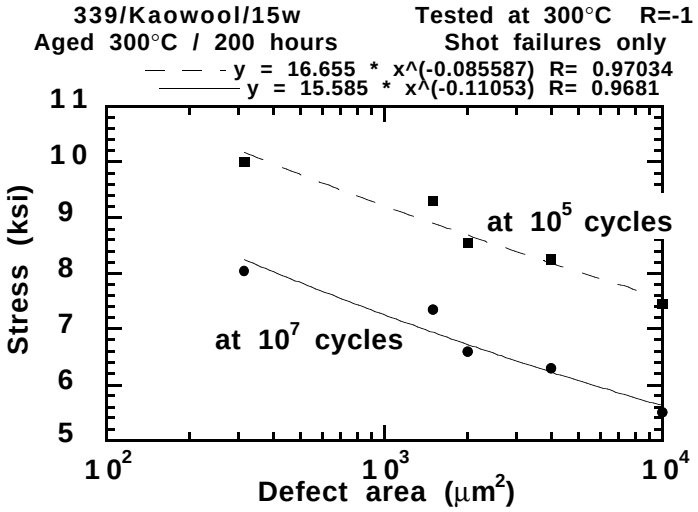

Fig. 27. Fatigue strength at 10^5 and 10^7 cycles versus defect area for 339/Kaowool/15w with failures due to shot particles at 300°C. Lines represent a power law fit to the data.

Life versus local stress intensity and predicted life versus experimental data are shown in Figs. 28 and 29 for the ten data points suitable for this analysis. In both these figures, more scatter is observed between experimental data and the predictions of the model than observed for shot and porosity defects at 200°C. An examination of the defect characteristics for the data in Figs. 28 and 29 reveals that four defects were not single, hollow shot particles. (In the analysis of shot particle failures at 200°C, all data points resulted from failure origins at single, hollow shot particles). These data points with complex failure origins are listed in Table II with the characteristics of the failure-initiating defect.

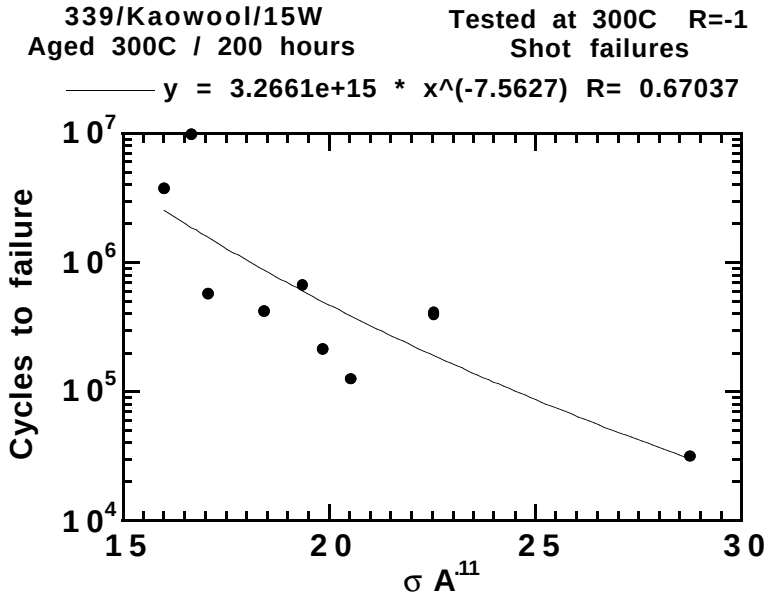

Fig. 28. Cycles to failure versus local stress intensity for shot failures at 300°C. Local stress intensity ($\sigma A^{.11}$) is derived from the analysis in Fig. 25. Line represents a power law fit to the data.

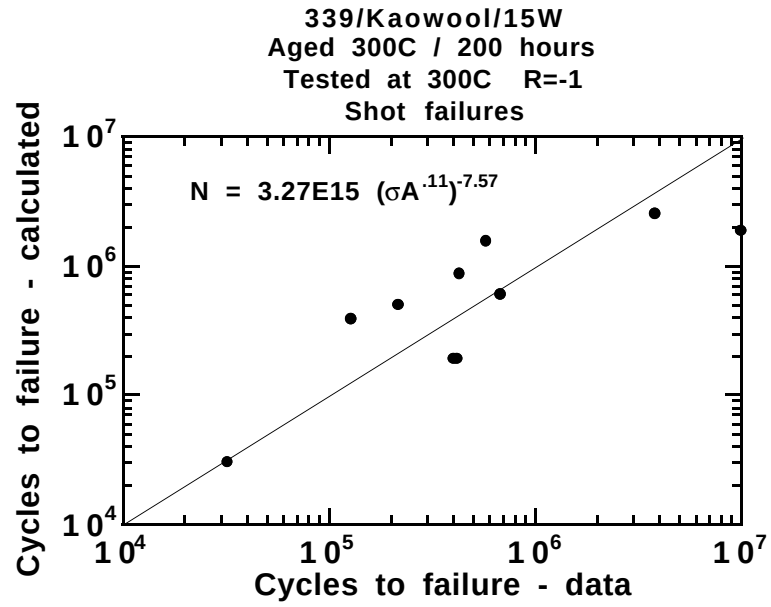

Fig. 29. Calculated number of cycles to failure versus experimental data. Calculations are based on the equation shown in the figure.

Table II
Defect Characteristics for Selected Data Points Tested at 300°C

Sample ID	Stress (ksi)	Cycles to failure	Defect Characteristics
C111392-126-3	8.5	4.14E5	Two particles together
C111392-125-3	8.5	3.98E5	Cluster of shot particles
C111392-128-3	8	5.76E5	Difficult to quantify; several shot particles
C051194-23-3	12	3.20E4	Filled shot

Figure 28 was re-plotted without the four data points shown in Table II and the results are shown in Fig. 30. Agreement with the proposed model is good; however, not as good as shown in Figs. 14 and 21 for the data at 200°C. The calculated life, using the equation obtained in Fig. 30, is compared to experimental data in Fig. 31. The life equations for the 339/Kaowool/15w composite with the three defect type / testing temperature combinations are shown in Table III.

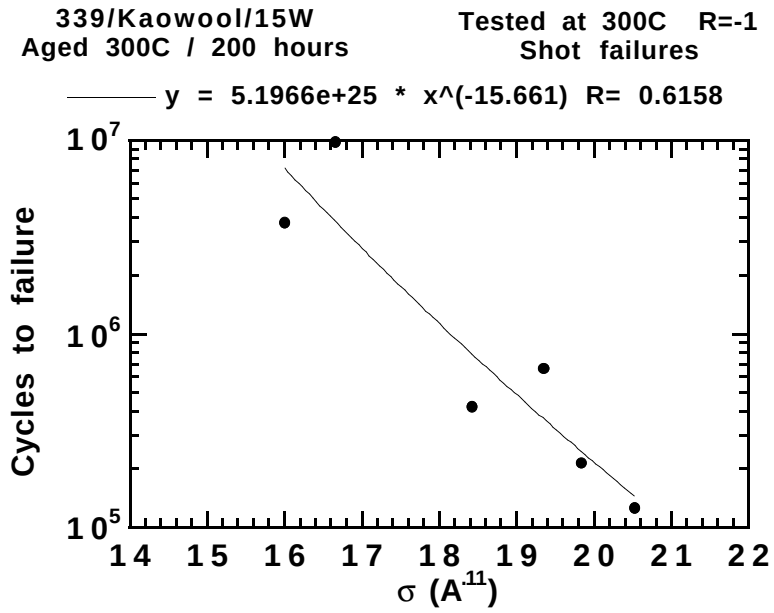

Fig. 30. Replot of data in Fig. 28 with suspect data points removed (see text).

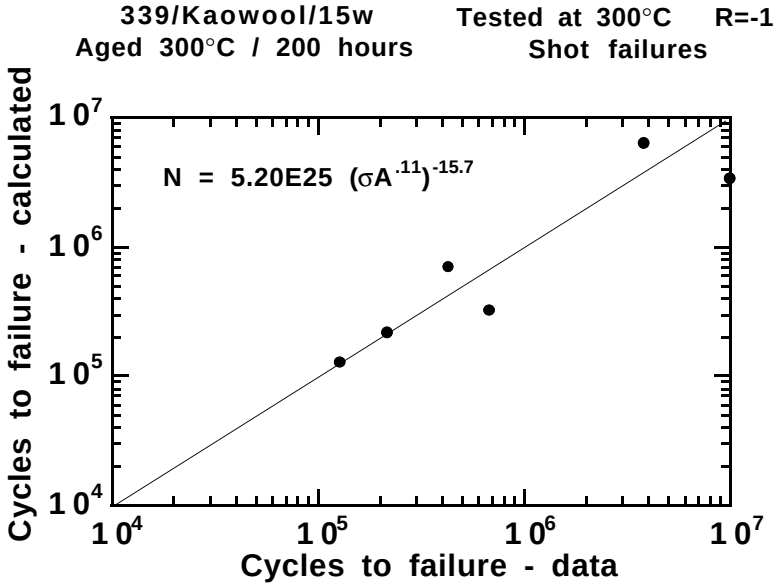

Fig. 31. Calculated number of cycles to failure versus experimental data. Calculations are based on the equation shown in the figure.

Table III
Life Equations for 339/Kaowool/15w
with Different Defect Types and Testing Temperatures

Defect type / testing temperature	Equation	Comments
shot particles / 200°C	$N = 3.83\ 10^{26}\ (\sigma A^{.15})^{-12.9}$	
shot particles / 200°C	$N = 1.17\ 10^{23}\ (\sigma A^{.077})^{-12.7}$	short defect data
porosity / 200°C	$N = 7.27\ 10^{28}\ (\sigma A^{.072})^{-17.2}$	
porosity / 200°C	$N = 2.85\ 10^{29}\ (\sigma A^{.041})^{-19.3}$	short defect data
shot particles / 300°C	$N = 3.27\ 10^{15}\ (\sigma A^{.11})^{-7.57}$	

MODEL PREDICTIONS

The model proposed and examined in the previous sections can be used to predict the σ-N behavior for 339/Kaowool/15W composites assuming that failures originate at known defects. The predicted σ-N curves for failures resulting from spherical shot particles at 200°C are shown in Fig. 32 for hollow particles with diameters equal to 50 μm, 20 μm and 10 μm. The results show that the endurance limit (stress at 10^7 cycles) increases from 10.3 ksi for defects with 50 μm diameter, to 11.8 ksi for defects with 20 μm diameter to 13.0 ksi for defects with 10 μm diameter. The analysis in Fig. 32 assumes, of course, that no other failure modes dominate. As the particles or other failure origins are made smaller and smaller, then other failure modes can intervene. In the limit, one would expect failures to originate in the matrix and the σ-N curve would be determined by microstructural features that control strength, such as the size and/or spacing of the particles and the inherent strength of the matrix (which can have its own reinforcing dispersion typical for aluminum alloys). An example of this transistion in failure modes (to a matrix dominated failure at small defect sizes) is provided in the next section for the case of SiC reinforced Al.

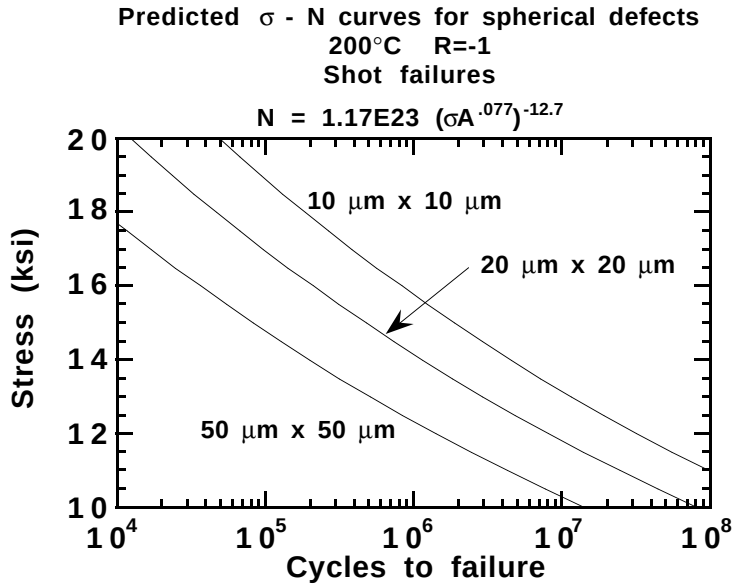

Fig. 32. Predicted σ - N curves for failures due to spherical shot particles at 200°C.

The model can also be used to study the σ-N behavior, when competing failure modes are present, for MMCs containing both shot and porosity. Predicted σ-N curves are shown in Fig. 33 for failures due to spherical shot particles (solid curves) and porosity (dotted curves) at 200°C. For both shot and porosity, two defect sizes were considered - 10 μm diameter and 50 μm diameter. Figure 33 shows that for 10 μm size defects, porosity is more damaging than shot. However, the difference between them decreses with decreasing stress and the two σ-N curves converge at 10^8 cycles. For the 50 μm diameter defects, porosity is more damaging than shot in the high stress / low life regime and shot is more damaging than porosity in the low stress / high life regime. The transistion from porosity-dominated failures to shot-dominated failures occurs at 2 10^6 cycles. As discussed previously, for large defects at comparable size, porosity is less damaging than shot. This conclusion is supported by the results in Fig. 33.

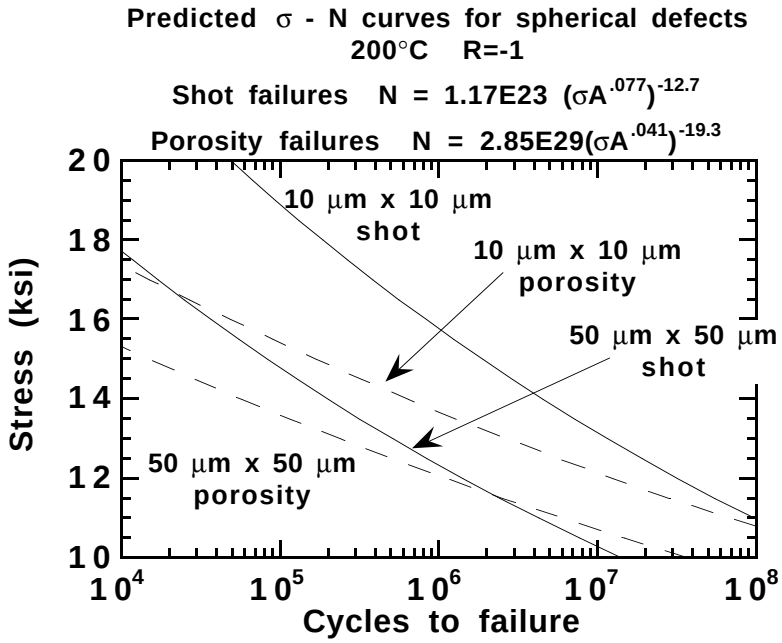

Fig. 33. Predicted σ -N curves for failures due to spherical shot (solid curves) and porosity (dashed curves) at 200°C

ANALYSIS OF DATA FROM THE LITERATURE

The literature contains very little data that can be used to assess the influence of defect size on fatigue life in MMCs. The one notable exception is from the work of Holcomb [9] on the 2124/SiC/20p composite. This material was processed from metal powders that were blended with particle powders containing three different average sizes - 3 μm, 17 μm and 35 μm. The powders were then consolidated, extruded and T6 treated (heat treated for 10 hrs. at 175°C). The samples were then fatigue tested under stress control at room temperature using smooth bar samples and R = -1. In the high cycle fatigue regime, failures often originated from fracture of the SiC particles. For the 17 and 35 μm particle samples, fatigue failures initiated predominatly from fractured SiC particles. For the 3 μm particle samples, fatigue failures were either associated with particle

fracture or failure in the matrix. Thus the 3 μm material appears to have a particle size in which a transistion is being made from particle-initiated failure (at large particle sizes) to matrix initiated failure (at small particle sizes).

The fatigue strength at 10^7 cycles for the 2124/SiC/20p composite (obtained from ref. 9) was then plotted versus defect area assuming failure originated from the SiC particles. The results are shown in Fig. 34. The area exponent was found to be 11.8, which is comparable to the values found for shot particles in the present study.

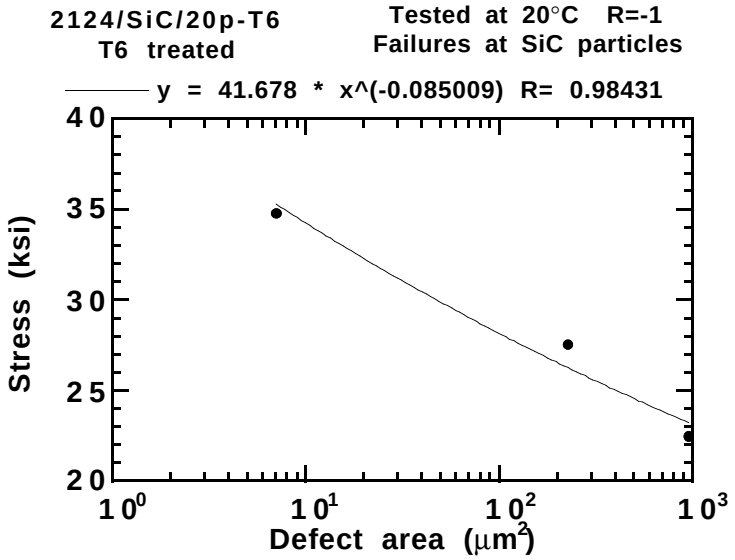

Fig. 34. Fatigue strength at 10^7 cycles versus defect area for 2124/SiC/20p-T6 at 20°C. Fatigue failures are assumed to initiate at SiC particles. Line represents a power law fit to the data. Fatigue data is from ref. 9.

SUMMARY AND CONCLUSIONS

The high cycle fatigue behavior has been studied for MMCs based on the aluminum 339 casting alloy with Kaowool reinforcement. This report describes results and data analysis for the 339/Kaowool/15w composite. The project involved testing 130 339/Kaowool/15w samples at different temperatures from room temperature to 300°C. Experiments were conducted on samples that had received different annealing treatments before testing. The defects responsible for fatigue failure were characterized. In the high cycle fatigue regime, the number of cycles to failure was found to vary as a power law function of the stress. Sufficient data were available for failures originating from three different defect / testing temperature combinations to quantify the relationship between defect type, defect size and cycling stress on resulting fatigue life. The three defect type / testing temperature combinations were shot particles at 200°C, porosity at 200°C and shot particles at 300°C. For all three combinations, the fatigue strengths at 10^5 and 10^7 cycles were found to follow a phenomenological relationship involving the stress and the cross-sectional area of the defect (shown as Equation (1)). The analysis follows a model derived by Murakami and Endo, in which the local stress intensity produced by a defect is related to the cross-

sectional area of the defect. The area exponent in Equation (1) was larger than expected from continuum mechanics calculations, indicating the local stress intensity was not as large as predicted by theory. This difference was attributed to a size scale effect. In addition for porosity failures, ligaments span the defect region and thus reduce the local stress intensity. A new model was proposed to predict the life of samples as a function of stress and defect characteristics (size and type). For the three data sets described above, the model could predict the life of the three different defect/temperature combinations described above to better than half a decade. Extension of the model to defect sizes smaller than observed in the current experiments provides insight into fatigue limits and σ-N behavior that might be expected with cleaner composites. For spherical hollow shot particles, the endurance limit (stress at 10^7 cycles) increases from 10.3 ksi for defects with 50 μm diameter, to 11.8 ksi for defects with 20 μm diameter to 13.0 ksi for defects with 10 μm diameter.

ACKNOWLEDGEMENTS

The authors acknowledge the work of Dave Hiromoto in mechanical testing and Jim Ferreira and Ed Sedillo for metallography and SEM fractography. This work was performed under the auspices of the U.S. Department of Energy by Lawrence Livermore National Laboratory under contract No. W-7405-Eng-48.

REFERENCES

1. D.R. Lesuer, T. G. Nieh, and C. K. Syn, “Fatigue of Metal Matrix Composites”, First year summary report, LLNL, 1994.

2. W.J. Baxter, presented at CRADA meeting, Nov. 16, 1993.

3. T.G. Nieh, D. R. Lesuer, and C. K. Syn, *Scripta Metallurgica et Materialia*, 1995, **32**, 707-712.

4. Y. Murakami and M. Endo, *International Journal of Fatigue*, 1994, **16**, 163 - 182.

5. Y. Murakami and M. Endo, *Engineering Fracture Mechanics*, 1983, **17**, 1 -15.

6. H. Nisitani and K. Kawano, *Transactions Japan Society of Mechanical Engineers*, 1971, **37**, 1492-1496.

7. Y. Murakami and T. Endo, in “The Effects of Small Defects on the Fatigue Strength of Hard Steels”, in *Proceedings of the International Conference on Fatigue ‘81*, Warweick University, 1981, 431-440.

8. S. Suresh, Fatigue of Materials, Cambridge University Press, 1991.

9. S.W. Holcomb, “The Effects of Particle Size on High Cycle Fatigue Properties of Silicon Carbide Reinforced 2124 Aluminum”, M.S. Thesis, University of Southern California, 1992.

			ISOTHERMAL UNIAXIAL FATIGUE							
Material	Temp (oC)	Sample ID & #	Stress (ksi)	#Cycles	Initiation Site	Defect Shape	Defect Size XxY (μm)	Defect Depth (μm)	Fatigue Zone Size (mm)	Comments
				Unreinforcd Matrix Alloy						
339	20	C120292-39-4	15	2.20E+04	I	Elong.	1000x2000	0-800	1.9	Unaged. Al rich/EDAX.
339	20	C120292-33-3	14	7.34E+05	P	Irreg.	540x540	0-520	2.3	Unaged.
339	20	C120292-67-5	14.5	1.20E+06	P	Irreg.	300x100	0	1	Unaged. EDAX.
339	20	C120392-33-4	13.5	1.80E+06	I	Elong	70x200	0-180	1.8	Unaged. EDAX.
339	20	C120392-29-3	13	1.49E+07 Runout						
					7% Kaowool					
339/Kao/7	20	C111392-31-1	31	4.00E+02	S	Elong.	50x150	0-120	Unmeas.	Unaged. 1 fract. surface examined.
339/Kao/7	20	C111392-31-3	20	4.10E+04	P/S	Elong	100x15 20x100	0	Unmeas.	Unaged. Shot on 1 surface, porosity on the other.
339/Kao/7	20	C111392-32-4	18.5	1.39E+05	S	Oval	50x70	0-70	1.5	Unaged. 2 fract. surf. exam. EDAX both Surf.
339/Kao/7	20	C111392-32-5	17	5.00E+05	S/P	Sickle	300	0	Unmeas.	Unaged. 2 fract. surfaces examined.
339/Kao/7	20	C111392-34-4	17	9.87E+06	S	Rctngl.	60x45	0-45	1.5	Unaged. EDAX one side.
339/Kao/7	20	C111392-31-2	15	1.01E+07 Runout						Unaged.
339/Kao/7	300	C111392-41-1	8.5	9.95E+04	S	2 elong. touch.	65x35 15	0-35	Unmeas.	300C/200h preaged. 2 touching elong. shots. 2 fract. surf's exam. EDAX.
339/Kao/7	300	C111392-45-1	8	3.80E+05	S/S	Spher. Elong.	40 100x45	0-45	1.5	300C/200h EDAX. A 2nd interpretation.
339/Kao/7	300	C111392-54-1	7.5	4.02E+05	S/P	Spher. Irreg.	25x45 45	0-35	1.5	300C/200h 2 fract. surfaces examined. EDAX done.
339/Kao/7	300	C111392-44-1	7	1.25E+06	S	Spher.	50	0-50	1.5	300C/200h
339/Kao/7	300	C111392-40-1	6.75	10M	S	Spher.	30x50		Unmeas.	300C/200h2 fract. surf. xm'ed. Origin difficult to establish.
339/Kao/7	300	C111392-55-1	6.5	10M+ Runout						

Material	Temp (oC)	Sample ID & #	Stress (ksi)	#Cycles	Initiation Site	Defect Shape	Defect Size XxY (μm)	Defect Depth (μm)	Fatigue Zone Size (mm)	Comments
					15% Kaowool					
339/Kao/15	20	C100292-30-7	17	8.82E+05	I	Elong	150x300	50		Unaged. CAT scan. before testing. Failed in grip.
339/Kao/15	20	C111392-116-2	17	8.57E+04	S	Spher.	40x50	2	1.5	Unaged.CAT scan. (200μm resol'n).
339/Kao/15	20	C111392-117-1	16	3.60E+05	S	Sickle	30x150	60	1.4	Unaged. CAT (50 & 200μm resol'n).
339/Kao/15	20	C111392-126-4	16	3.27E+04	P	Irreg.	60x80	0-80	1.4	300°C/200hrs preaged.
339/Kao/15	20	C111392-130-1	15	1.86E+06	S/P	Spher. Irreg.	50 40x130	60/ 30-100	1.2	Unaged. Shot at the tip of an oblique chain of porosity.
339/Kao/15	20	C111392-116-2	15	3.92E+05	P	Irreg.	260x20	30-170	1.6	
339/Kao/15	20	C111392-120-2	15							Unaged. CAT (50 & 200μm resol'n). Failed in grip before testing.
339/Kao/15	300	C100292-36-3	8.5	3.78E+06	S	Cluster of shots	<20	50	1.8	300C/200h preaged. CAT scan. 50μm resol'n
339/Kao/15	300	C111392-128-4	8.5	6.72E+05	S	Spher.	50x45	0-45	1.9	300C/200h
339/Kao/15	300	C111392-126-3	8.5	4.14E+05	S	Bagel	60x150	0-60	1.5	300C/200h preaged. Bagel-shaped
339/Kao/15	300	C111392-128-7	8.5	2.61E+05	P	Two chains	400x150	10-140	1.4	300C/200h preaged. Two connected subsurface chains
339/Kao/15	300	C111392-125-3	8.5	3.98E+05	S	Spher.	120x75	0	1.2	300C/200h preaged. Cluster of small shots
339/Kao/15	300	C111392-114-2	8.5	7.31E+04	P	Cluster of Irreg.	250x250	50	1.2	300C/200h preaged. Cluster of six small porosities of about 50x30.
339/Kao/15	300	C111392-131-4	8	2.49E+06	I	Irreg.	40x15	0	1.8	300C/200h preaged. Sp. w/Baxter
339/Kao/15	300	C111392-128-3	8	5.76E+05	S	Elong.	25x50	0-50	1.3	300C/200h preaged. Several small shots.
339/Kao/15	300	C111392-120-1	8	4.25E+05	S/S	Spher. Spher.	50 80	250 >250	Im-meas'ble	300C/200h preaged . CAT scan. 50 μm resol' Shot possible origin.
339/Koa/15	300	C111392-114-3	8	2.16E+05	S	Spher.	70	0-60	1.7	300C/200h preaged.
339/Koa/15	300	C111392-129-7	8	1.84E+05	P	Irreg.	40x300	20-200	1.7	300C/200h preaged. Multiple long-chain
339/Koa/15	300	C111392-128-6	8	1.66E+05	P	Irreg.	30x150	30-150	1.6	300C/200h preaged. Two straight chains.
339/Kao/15	300	C111392-116-1	8		P	Irreg.				Failed at start.
339/Kao/15	300	C110292-36-2	7.5	10MC+	Runout	-	-	-	-	300C/200h preaged. CAT scan. (50μm resol'n)
339/Kao/15	300	C111392-129-3	7.5	9.87E+06	S	Spher.	20x90	100	1.6	300C/200h preaged. Shot partially hollow.
339/Koa/15	300	C111392-129-4	7.5	4.34E+06	I	Irreg.	20x240	0-60	1.7	300C/200h preaged. Elliptic chain of incl. & shots

Material	Temp (oC)	Sample ID & #	Stress (ksi)	#Cycles	Initiation Site	Defect Shape	Defect Size XxY (μm)	Defect Depth (μm)	Fatigue Zone Size (mm)	Comments
339/Kao/15	300	C111392-131-1	7.5	2.06E+06	P	Irreg.	120	0	1.4	300C/200h preaged. CAT Scan. (50 μm resol'n). Maybe unpre-annealed
339/Kao/15	300	C111392-131-3	7.5	6.25E+05	P	Irreg.	450	0	1.3	300C/200h preaged. CAT scanned 50 μm resol'n.
339/Kao/15	300	C111392-118-2	7.5	1.27E+05	S+P S	Irreg. Spher.	75x160 70	30-190 1000	1.0?	300C/200h preaged. CAT Scan. (50 μm resol'n)
339/Koa/15	200	C111392-127-4	13	3.46E+05	S	Thumb	40x100	0-100	1.1	200C/200h preaged. High aspect ratio. Sp. w/Baxter
339/Koa/15	200	C111392-124-3	13	2.44E+05	S	Peach	30x70	0-60	1	200C/200h preaged. Partially filled.
339/Kao/15	200	C111392-125-4	13	2.27E+05	S	Shper.	80x40	0-40	1	200C/200h preaged. Sp. w/Baxter
339/Kao/15	200	C111392-124-4	13	1.32E+05	P	Irreg.	70x50	0-70	1	200C/200h preaged.
339/Kao/15	200	C111392-118-1	13	4.98E+04	P	Irreg.	150x200	0-200	1	200C/200h preaged. CAT scanned.
339/Koa/15	200	C111392-118-3	12	1.97E+06	S	Ellips.	70x40	0	1	200C/200h preaged. Sp. w/Baxter
339/Koa/15	200	C111392-128-5	12	4.14E+05	P	Irreg	80x200	0-80	1.4	200C/200h preaged. ORNL sp., multiple sites. 4 additinal clusters nearby.
339/Kao/15	200	C111392-120-4	12	3.94E+05	P/S	Irreg.	70x90/ 60x35	0-70/30	1.2	200C/200h preaged. Two sites 300 μm apart.
339/Kao/15	200	C111392-131-2	12	2.97E+05	S	Spher.	80x100	10-110	1.2	200C/200h preaged. Sp. w/Baxter
339/Kao/15	200	C111392-120-3	12	2.91E+04	P	Irreg.	100x350	10-100	1	200C/200h preaged.
339/Kao/15	200	C111392-123-3	11	4.72E+06	S	Apple	80	0	1.8	200C/200h preaged. Shot fractured in halves.
339/Kao/15	200	C111392-118-4	11	4.08E+06	S P	Irreg. Irreg.	35x50/ 100x30	10-25/ 50-100	1.8	200C/200h preaged. Shot and long fibers. /Oblique porosity chain.
339/Kao/15	200	C111392-114-1	11	2.50E+06	P	Irreg.	130x80	0-80	1.2	200C/200h preaged. Interconnected porosity.
339/Kao/15	200	C111392-114-4	10	1.08E+07	P	Irreg.	90x140	0-90	1.6	200C/200h preaged. C-shaped chain of porosity
339/Kao/15	200	C111392-117-2	10	4.64E+06	P	Irreg.	120x1500	0-120	1.5	200C/200h preaged. Interconnected porosity.
339/Kao/15	200	C111392-123-4	9	10M+	Runout	-	-	-	Im-meas-urable	200C/200h preaged. Cracks detected on surface shots and fibers. Out for Synchrtron Rad. CAT. by Tom Breunig-Sandia Lab
339/Kao/15	200	C111392-130-2	9	10M+	Runout S	Spher.	100	0	1	200C/200h preaged. CAT scanned. Pulled to fail. at RT after fatigue testing; UTS=29.4ksi. Unaged.

Material	Temp (oC)	Sample ID & #	Stress (ksi)	#Cycles	Initiation Site	Defect Shape	Defect Size XxY (µm)	Defect Depth (µm)	Fatigue Zone Size (mm)	Comments
				15% Kaowool / Low Shot						
339/Kao/15	300	C051194-29-2	14	4.95E+03						Aged 300C/200hr. New batch.
339/Kao/15	300	C051194-25-3	14	6.42E+03						Aged 300C/200hr. New batch.
339/Kao/15	300	C051194-17-3	14	2.35E+04	S	Irreg.	75x20	0-20	1	Unaged. New batch. Preform macro-crack on shlder & gage. Solid shot.
339/Kao/15	300	C051194-17-6	12	1.13E+05	S	Spher.	25	80	1	Unaged. New batch. Preform crack on shlder & gage. Solid shot.
339/Kao/15	300	C051194-27-3	12	1.12E+05	S	Spher.	40	0	1.2	Unaged. New batch. Solid shot.
339/Kao/15	300	C051194-23-2	12	4.21E+04	S	Spher.	60	0-70	1	Unaged. 3rd batch. Hollow shot.
339/Ka0/15	300	C051194-23-3	12	3.20E+04	S	Oval	55x65	0-55	1	Preaged 300C/200hr. 3rd batch. Hollow shot filled w/matrix.
339/Kao/15	300	C051194-27-4	11	7.59E+04	S	Spher.	65	3	1.2	Unaged. New batch. Preform macro-crack on shlder. Solid shot.
339/Kao/15	300	C051194-29-1	11	4.94E+04						Aged 300C/200hr. New batch.
339/Kao/15	300	C051194-15-2	10	1.22E+06	S	Peach	81x72	3.0-75	1.5	Preaged 300C/200hr. 3rd batch. Solid shot. Tester untripped on fail. Retest recommended.
339/Kao/15	300	C051194-27-5	10	1.15E+06	Fiber	Fiber	50x10	0-10	1.3	Unaged. New batch. Preform crack on shoulder. Fiber doublet.
339/Kao/15	300	C051194-32-3	10	1.12E+06	S	Spher.	15	15	0.86	Unaged. Small shots cluster. Cluster 30 µm size & 0 depth.
339/Kao/15	300	C051194-15-5	10	2.57E+05	S	Irreg.	60x180	0-80	1.25	Unaged. 3rd batch. Shot surface x-section ~70 µm.
339/Kao/15	300	C051194-22-4	9.5	2.68E+05	S	Irreg,	70x60	0-60	1.6	Unaged.
339/Kao/15	300	C051194-32-6	9	3.00E+06	S & Fiber	Irreg.	30	3.0-30	1.5	Unaged. Cluster of small shots & fibers.
339/Kao/15	300	C051194-27-6	9	1.53E+06	S	Irreg. Cluster	50x70 50x50	0-50	1.25	Unaged. New batch. Pre-form crack on shoulder & gage.
339/Kao/15	300	C051194-25-1	9	6.02E+05						300C/200hr.
339/Kao/15	300	C051094-25-2	9	3.32E+05	Powder cluster & I(R)	Irreg. & Rod	400x200 90x15	0-200 0-80		300C/200hr.
339/Koa/15	300	C051194-21-2	8.5	4.26E+06	I?	Irreg.	20x20	0	2	Unaged.
339/Koa/15	300	C051194-32-5	8.5	3.40E+06	I or S	Irreg.	10x30	4	2	Unaged.

Material	Temp (oC)	Sample ID & #	Stress (ksi)	#Cycles	Initiation Site	Defect Shape	Defect Size XxY (μm)	Defect Depth (μm)	Fatigue Zone Size (mm)	Comments
339/Kao/15	300	C051194-21-5	8	8.36E+06	Unid'ble	N/A	N/A	N/A	2.1	Unaged.
339/Kao/15	300	C051194-16-2	8	8.24E+06	S	Irreg.	18-Dec	35-50	1.6	Unaged. 3rd batch. Preform crack on shldr & gage.
339/Kao/15	300	C051194-22-1	8	7.82E+06	S	Spher.	20x10	10	2.5	Unaged.
339/Kao/15	300	C051194-16-4	8	2.45E+06	Unid'ble	N/A	N/A	N/A	N/A	Preaged 300C/200hr. 3rd batch. Test interrupted @1.65MC cycles .
339/Kao/15	300	C051194-32-1	7.5	10MC Runout	N/A	N/A	N/A	N/A	N/A	Unaged. Out for Syncrton. Rad. CAT by Tom Breunig-Sandia. Lab.
339/Koa/15	300	C051194-21-4	7.5	6.32E+06	S S	Spher. Spher.	80x10 15	60 25	2.6	Unaged. 3 small shots, separate but adjacent.
339/Kao/15	300	C051194-29-4	7	10MC Runout						Preaged 300C/200hr.
339/Kao/15	200	C051194-27-1	17	4.59E+04	S	Spher.	80	0	1	Unaged. New batch from WB. Partly solid shot filled w/matrix.
339/Kao/15	200	C051194-17-5	16	8.33E+04	S	Oval	110x35	0	1	Unaged. New batch. Preform crack on shlder & gage. Solid shot.
339/Kao/15	200	C051194-15-3	16	2.52E+04	S	Irreg.	58x68	15-84	1.2	Preaged 200C/200hr. 3rd batch. Hollow shot.
339/Kao/15	200	C051194-16-3	16	5.49E+03	I	Hemi-sph.	200x100	0-100	1	Preaged 200C/200hr. 3rd batch. Inclusion and fine-grained matrx area. Probably thinskinned shot.
339/Kao/15	200	C051194-21-3	15	2.05E+05	S	Irreg.	85x50	0-50	1.2	Unaged.Spherical shot with tail.
339/Kao/15	200	C051194-17-4	14	1.13E+06	S	Irreg.	50x90	0-90	1	Unaged. New batch. Preform crack on shoulder. Solid shot.
339/Kao/15	200	C051194-22-2	14	5.14E+05	S	Spher.	100x50	0-50	1.4	Unaged. Half-solid, half filled w/ fragments.
339/Kao/15	200	C051194-23-6	14	1.36E+05	S	Spher.	65	0-65	1	Preaged 200C/200hr. 3rd batch. Hollow w/2μ wall thickness.
339/Kao/15	200	C051194-23-4	14	1.22E+05	S	Gourd	52x80	0-70	1.25	Preaged 200C/200hr. 3rd batch.
339/Koa/15	200	C051194-32-2	13	1.87E+06	S	Irreg.	30x30	6	1.6	Unaged. Chain (Elliptic, 130x180) of shots (5 to 10 x 20 to 60 μm).
339/Kao/15	200	C051194-22-3	13	8.44E+05	S	Elliptic	50x60	0	1.6	Unaged. Same. Partly hollow shot.
339/Kao/15	200	C051194-21-1	12	6.04E+06	S	Elliptic	6x15	10	1.25	Unaged. Same.
339/Kao/15	200	C051194-22-5	12	9.08E+06	S	Spher.	50	5	1.75	Unaged. Same. Partly hollow shot.
339/Kao/15	200	C051194-27-2	12	1.66E+06	n/a	n/a	n/a	n/a	n/a	Unaged. New from WB. Pre-form crack on shoulder & gage.
339/Kao/15	200	C051194-15-1	12	1.22E+06	S	Irreg.	60x55	Feb-57	1.5	Preaged 200C/200hr. 3rd batch. Solid shot.

Material	Temp (oC)	Sample ID & #	Stress (ksi)	#Cycles	Initiation Site	Defect Shape	Defect Size XxY (μm)	Defect Depth (μm)	Fatigue Zone Size (mm)	Comments
339/Kao/15	200	C051194-16-5	12	8.10E+05	S	Irreg.	50x70	0-70		Preaged 200C/200hr. 3rd batch. Hollow filled.
339/Kao/15	100	C051194-25-4	14	4.20E+04						Aged 300C/200hr. New batch.
339/Kao/15	100	C051194-29-3	14	3.83E+04						Aged 300C/200hr. New batch.
339/kao/15	25	C051194-15-6	18	2.81E+05	S	Irreg.	55x120	0-120	1.2	Unaged. 3rd batch.
339/Kao/15	25	C051194-17-2	18	1.44E+05	S	Irreg.	70x25	0-50	1	Unaged.New batch. Preform crack on shlder & gage. Solid shot. Thick fibers nearby.
339/Kao/15	25	C051194-23-5	17	2.29E+06	S	Irre..	50x66	0-66	1	Unaged. 3rd batch. Many fibers nearby.
339/Kao/15	25	C051194-17-1	17	1.44E+05	S	Irreg.	20x130	0-90	1.1	Unaged. New batch. Preform crack on shoulder & gage. Fiber-like shot. Same length fiber nearby.
339/Kao/15	25	C051194-16-1	17	1.40E+05	S	Spher.	65x50	0-50	1.2	3rd batch. Unaged.
339/Kao/15	25	C051194-32-4	17	1.34E+05	S	Irreg.	100x150	0-150	1	Unaged.
339/Kao/15	25	C051194-21-6	16	1.39E+07	Runout					Unaged.
339/Kao/15	25	C051194-15-4	16	9.30E+04	S	Spher.	80x100	0-80	1.25	Unaged. 3rd batch. Preform crack on gage & shlder.
339/Kao/15	25	C051194-23-1	16	8.98E+04	Fiber	Elong.	200x12	0-45	1.2	Unaged.

Material	Temp (oC)	Sample ID & #	Stress (ksi)	#Cycles	Initiation Site	Defect Shape	Defect Size XxY (μm)	Defect Depth (μm)	Fatigue Zone Size (mm)	Comments
				15% Kaowool / Didier Cleaned						
339/Kao/15	300	C051094-45-1	12	6.31E+04	R	Elong.	45x25	0-25		300C/200hr. Multi-grain shot w/o clean facets.
339/Kao/15	300	C051094-45-3	11	9.00E+04	Powder Cluster	Oval	45x27	0-27		300C/200hr. Pouch of of un-sintered particles & partially glazed 3 layer skin, upto 10 μm thick.
339/Kao/15	300	C051094-44-2	10	2.85E+05	I & Fiber	Oval fiber	15x10 100x6	65-75 120-190		300C/200hr. Source area abundant w/other small defects.
339/Kao/15	300	C051094-42-1	10	3.20E+05	I	Irreg.	55x28	0-28		300C/200hr. Solid incl'sn.
339/Kao/15	300	C051094-49-1	9	1.01E+06	I	Potato	100x42	3500	2	300C/200hr. Incls'n near the center. Incl's'sn w/internal cracks.
339/Kao/15	300	C051094-59-06	1.7-17	2.43E+03						300C/200hr. ***R=0.1***
339/Kao/15	300	C051094-58-3	1.2-12	9.61E+05						300C/200hr. ***R=0.1***
339/Kao/15	275	C051094-48-5	13	1.40E+04	R	Fiber	20x85	0-65		300C/200hr. Surf dim. 50μ.
339/Kao/15	250	C051094-48-3	13	5.38E+04	R	Fiber				300C/200hr. Source area abundant w/small shots(?) & fibers.
339/Kao/15	225	C051094-47-2	13	3.60E+04	R	5-gon	110-70	550		300C/200hr. Huge subsurf. Defect.
339/Kao/15	225	C051094-49-2	13	4.33E+04	R	Equiaxed	15x15	10.0-25		300C/200hr.
339/Kao/15	200	C051094-47-5	16	2.23E+04	R	Elong.	60-16	0-25		200C/200hr. 2 // long shots. Surface dim's'n 50 μm.
339/Kao/15	200	C051094-49-3	15	5.11E+04	R	Fiber	150x20	0-30		200C/200hr. Defect surf.exposed -0-.
339/Kao/15	200	C051094-49-5	14	1.64E+05	R	Fiber	105x6	0-8		200C/200hr. Surf dim. 45μ.
339/Kao/15	200	C051094-48-1	13	3.57E+05	R	Elong.	90-30	0-75		200C/200hr. Long tapered. Surface dimesion 70 μm.
339/Kao/15	200	C051094-48-2	12	9.80E+05	Powder cluster	Egg	55x30	0-50		200C/200hr. Incompletely sintered powder cluster. Surf dim 15 μm.
339/Kao/15	200	C051094-47-4	11	5.78E+06	R or I	Spher.	50x37	0-37		200C/200hr. Solid. Multi-fracture. Surf dim 50μm.
339/Kao/15	200	C051094-59-3	15	1.27E+04						250C/200hr.
339/Kao/15	200	C051094-59-1	13	1.09E+05						250C/200hr.

Material	Temp (oC)	Sample ID & #	Stress (ksi)	#Cycles	Initiation Site	Defect Shape	Defect Size XxY (µm)	Defect Depth (µm)	Fatigue Zone Size (mm)	Comments
339/Kao/15	200	C051094-59-5	11	7.06E+05						250/200hr.
339/Kao/15	200	C051094-45-2	12	1.26E+05	R	Elong.	105x23	0-30		300C/200hr. Long elongated shot.
339/Kao/15	200	C051094-44-1	11	3.79E+05	Powder cluster	Irreg.	40x30	10.0-50		300C/200hr. Pocket of incomplete sinter.
339/Kao/15	200	C051094-44-3	10	1.33E+06	R	Fiber	85x3	0-60		300C/200hr. Init. area abundant w/other fibers & incl's.
339/Kao/15	200	C051094-42-3	10	8.79E+05	I	Irreg.	25x15	0-15		300C/200hr. Fibers & a larger incls'n nearby.
339/Kao/15	175	C051094-49-4	13	8.45E+05	R or I	Elliptic	110-60	Center		200C/200hr. Multiple fract.
339/Kao/15	150	C051094-47-3	13	8.15E+04	R	Flake	110-20	130-150		300C/200hr
339/Kao/15	125	C051094-47-1	13	5.26E+04	R	Elong.	90x17	0-30		300C/200hr. Surf dim 50µm.
339/Kao/15	100	C051094-48-4	13	1.18E+05	R	Elong.	80-20	0-30		300C/200hr. Surf dim 25µm.
339/Kao/15	100	C051094-58-4	1.2-12	10M+ runout						300C/200hr. ***R=0.1***
339/Kao/15	100	C051094-42-4	12	2.29E+05	R	Elong.				300C/200hr. Source area rich w/ small shots & fibers.
339/Kao/15	100	C051094-45-4	11	1.01E+06	I	Irreg.	55x15	0-15		300C/200hr. Large incl. @ source and fibers nearby.
339/Kao/15	100	C051094-42-2	10	9.7E+06 Runout						300C/200hr. Stopped @9.7MC.
339/kao/15	100	C051094-44-4	10	10MC+ Runout						300C/200hr.
					R: Reinforrcement material.					

Technical Information Department • **Lawrence Livermore National Laboratory**
University of California • Livermore, California 94551